Synthesis of fluorescent G-quadruplex DNA binding ligands for the comparison of terminal group effects in molecular interaction: phenol versus methoxybenzene

Jingwei Jin[b,d‡], Jinqiang Hou[c,‡],Wei Long[d], Xinyue Zhang[b], Yu-Jing Lu[d], Dongli Li[b], Kun Zhang[b], and Wing-Leung Wong[a,b,*]

[a] The State Key Laboratory of Chemical Biology and Drug Discovery, Department of Applied Biology and Chemical Technology, The Hong Kong Polytechnic University, Hung Hom, Kowloon, Hong Kong, China.

[b] School of Biotechnology and Health Sciences, Wuyi University, Jiangmen 529020, P.R. China; and International Healthcare Innovation Institute (Jiangmen), Jiangmen 529040, P.R. China.

[c] Department of Chemistry, Lakehead University and Thunder Bay Regional Health Research Institute, 980 Oliver Road, Thunder Bay, On, P7B 6V4, Canada.
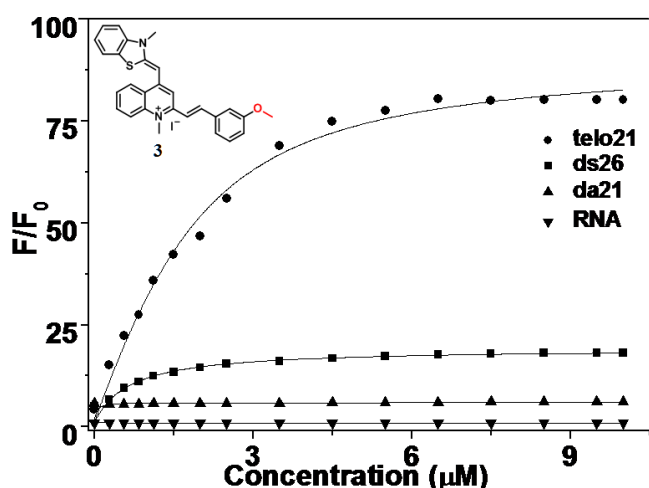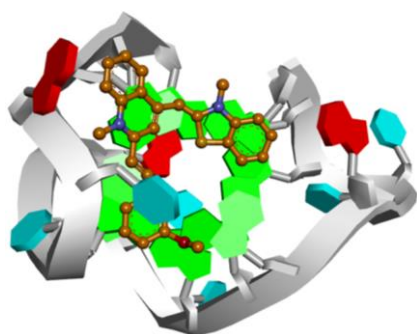
[d] Institute of Natural Medicine and Green Chemistry, School of Chemical Engineering and Light Industry, Guangdong University of Technology, Guangzhou 510006, P. R. China.

‡ The authors contributed equally to this work.

* Corresponding author
E-mail: wing.leung.wong@polyu.edu.hk

Graphical abstract

Abstract

A number of new fluorescent nucleic acid binding ligands were synthesized by utilizing the non-specific thiazole orange dye as the basic scaffold for molecular design. Under simple synthetic conditions, the molecular scaffold of thiazole orange bridged with a terminal side-group (phenol or methoxybenzene) becomes more flexible because the ethylene bridge is relatively less rigid than the methylene one of thiazole orange. It was found that these molecules showed better selectivity towards G-quadruplex DNA structure in molecular interactions with different type of nucleic acids. The difference in terms of induced DNA-ligand interaction signal, selectivity and binding affinity of the ligands with the representative nucleic acids including single-strand DNA, double-stranded DNA, telomere and promoter G4-DNA and ribosomal RNA were investigated. The position of the terminal methoxyl groups was found showing strong influence both on binding affinity and fluorescent discrimination among 19 nucleic acids tested. The ligand with a methoxyl group substituted at the *meta*-position of the styryl moiety exhibited the best fluorescent recognition performance towards telo21 G4-DNA. A good linear relationship between the fluorescent binding signal and the concentration of telo21 was obtained. The comparison of ligand-DNA interaction properties including equilibrium binding constants, molecular docking, G4-conformation change and stabilization ability for G4-structures was also conducted. Two cancer cell lines of PC3 (human prostate cancer cell) and hepG2 (human hepatoma cell) were selected to explore the inhibitory effect of the ligands on the cell growth. The IC_{50} values obtained in the MTT assay for the two cancer cells were found in the range of 3.4–10.8 μM.

Keywords: Fluorescent molecule; Thiazole orange derivative; G-quadruplex DNA binding ligand; DNA-ligand interaction.

Introduction

To advance the analytical technology in the field of biological and biomedical sciences, the development of fluorescent molecules that functions as effective tools for bio-recognition, bio-labeling, and imaging agents targeting important biomolecules including amino acids, nucleic acids, peptides, proteins, and biomarkers of cancers *in vivo* is important.[1-6] The wonderful imaging techniques, in the visible to near infrared regions, demonstrated with novel fluorophores and nano-materials such as green fluorescent proteins, nanoparticles and quantum dots, and organic dyes have been developed over the last few years. Fluorescence imaging is a non-invasive and sensitive tool for the investigation of biological functions of biomolecules and probing the molecular dynamics in live cells with the high brightness and photostability fluorescent compounds.[7-20] Currently, the selective sensing or detection of a particular type of biomolecules in their native environment such as in a living cell is still challenging.[21,22] For example, in the field of nucleic acid research, the discrimination of G-quadruplex DNA (G4-DNA) structures from other types of DNA molecules via fluorescent recognition method remains a challenge.[23-25] It is because the double stranded DNA substrates, which are more abundant in bio-systems, usually show strong binding affinity with small ligands or probes and cause poor discrimination. Therefore, many efforts are continuously being made to discover merit fluorescent G-quadruplexes specific binding ligands for live cell imaging.

It is interesting that the secondary structures of G4-DNA is distinctively different from the canonical double helix DNA and possess unique physical properties and biological functions. A number of literatures have reported that the design of molecules or binding ligands that fit the structural geometry of the G4-DNA secondary structures is a promising strategy to establish G4-specific fluorescent probes.[26-29] Our recent investigations also demonstrated that small molecules could achieve good fluorescence discrimination ability towards G4-DNA structures against other type of nucleic acids including duplex DNA and RNA and show strong emissive interaction signal.[30,31] Some factors such as the symmetry, the electronic effects and the characteristics of the terminal functional groups of the ligands have been known to influence

strongly the binding affinity and discrimination signal in many examples.[32-34] In recent years, a number of thiazole- and styryl-based fluorescent ligands that showed good fluorescence sensing performance towards G-quadruplex nucleic acids have been reported.[35-37]. However, the study to compare the polar terminal hydroxyl group with the non-polar methoxyl group based on the thiazole orange-modified ligand system in G4-DNA binding has not been studied. Some recent studies have compared the functional group of methoxybenzene and its corresponding phenol group of certain natural products, such as curcuminoids (interacting with human serum albumin)[38], flavonoids (interacting with PDIA3)[39] and resveratrol (interacting with TOPOII–DNA interface)[40] and revealed that the methoxyl groups exhibit interesting structure-activity relationship but their parental phenol groups do not have. Considering the character of the functional groups, methoxybenzene and phenol, the methoxyl groups can only act as a hydrogen bond acceptor and not a donor, while phenol can act both as donor and acceptor. In addition, compared with phenol, the methoxybenzene group is less polar and is more electron donating. These properties of the functional groups may be a feature of binding ligands that are capable of inducing different interaction behavior in the binding sites of protein or DNA to provide specific biofunction.

In the present study, we synthesized a series of nucleic acid binding ligands, which were designed with a terminal functional group of phenolic hydroxyl or methoxybenzene to understand their functional differences in the fluorescent signaling of interaction, selectivity, binding affinity and the ligand-DNA complex stabilization with nineteen nucleic acids including single-strand DNA, double-stranded DNA, telomere and promoter G4-DNA, and RNA. Moreover, by applying these G4-DNA binding ligands to live cancer cells of PC3 (human prostate cancer cell) and hepG2 (human hepatoma cell), the cytotoxicity in the range of 3-11 μM was observed.

Results and discussion

The fluorescent nucleic acid binding ligands (Figure 1: **1-4**) constructed based on the molecular skeleton of thiazole orange were synthesized through the condensation reaction of an

4

suitable aromatic aldehyde and the methyl group at the *ortho*-position of the 1-methylquinolinium scaffold with 4-methylpiperidine as a base in *n*-butanol under reflux conditions (Figure 1).[41] The ligands synthesized are able to form a π–conjugated molecular structure, in which the core fragment of methylquinolinium moiety bonds with a functionalized phenyl group through a relatively flexible ethylene bridge at the 2-position and also bonds with a benzothiazole through a relatively rigid methylene bridge at its 4-position. The overall structure of the ligands is therefore flexible and freely rotatable in solution. The isolated yields of these compounds were 81-89 %. The ligands were fully characterized with ^{1}H and ^{13}C NMR and mass spectrometry. The purity of the ligands was determined by HPLC before utilizing in the nucleic acid binding studies and bioassays.
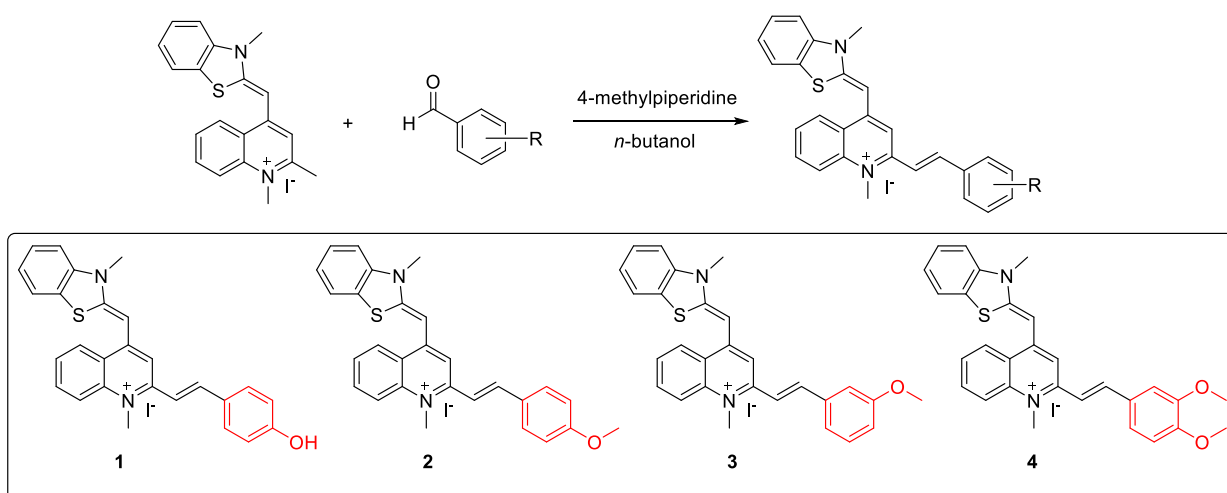

Figure 1. The synthetic route and the molecular structures of the fluorescent DNA binding ligands **1-4** synthesized for the comparison of interaction property.

The ligands are almost not emissive in solution due to the freely rotation property of the molecular fragments causing radiationless decays in excited electronic states of the molecules. However, when the rotation around the bonds of the methylene and ethylene bridges between the π–conjugated aromatic systems is restricted, it results the termination of the non-radiative decay channel[42] and thus the fluorescence signal of the ligands is restored. The fluorescence signal of the ligands is therefore sensitive to the rigidity of the environment. As demonstrated in Figure S1, the ligands dissolved in a mix-solvent system of glycerol in water (v/v %), in which altering the

water-glycerol ratio to regulate the viscosity of the medium, to observe the fluorescence signal changes. In the ligands tested, it was found that the induced fluorescence intensity reached maximum in 100 % glycerol medium due to the ability of molecular rotation is significantly restricted in the viscous glycerol. This indicates that the ligand upon binding to DNA is able to suppress the radiationless decays due to the high barrier for intramolecular torsional motion and thus induce a detectable fluorescence signal in both *in vitro* and *in vivo*.

The spectroscopic property, fluorescent signal changes, and binding affinity of the dyes were investigated with various DNA substrates in a Tris-HCl buffer solution at room temperature. The UV-vis absorption energy (λ_{max}) of these new dyes are in the range of 506-527 nm (major peak) and their emission maxima upon bound with the G-quadruplex DNA (G4-DNA) are located in the range of 530-624 nm, which is slightly red-shifted compared with thiazole orange (532 nm). In the fluorescence assays, a variety of nucleic acids including single stranded DNA (dt21, da21), double stranded DNA (4a4t, 4at, ds12, ds12), and G4-DNA (telomere DNA: htg22, telo21, 4telo, human12, oxy12, oxy28; promoter DNA: pu27, bc12, pu18, VEGF, RET, cik-1, ckit-2) were examined with ligands (**1**-**4**) to screen out which substrate could induce significant fluorescence signal. The fluorescence intensity enhanced may indicate the *in vitro* ligand-DNA interactions and could be compared for their target specificity. Form the fluorescence titration results, the G4-DNA substrates, particularly the telomeric G4-DNA, gave the highest fluorescence signals while the dsDNAs were found much less effective. The ssDNA substrates were also found very weak. Taking together, the ligands exhibited the highest preference towards telomeric G4-DNA under the same conditions (Figure 2). Moreover, the fluorescence intensity enhancement contributed from the interaction of ligand-telomeric G4-DNA was found in the order of **1** > **2** > **3** > **4**.

To compare the discrimination ability of the binding ligands towards different classes of nucleic acids, one representative substrate from each class including telo21 (G4-DNA), ds26 (double-stranded DNA), da21 (single-stranded DNA) and RNA was selected for the investigation. From Figure 3, the fluorescence titration experiments showed that the ligands have much higher

6

binding selectivity, in terms of enhanced interaction signals (F/F$_0$), towards telo21 G4-DNA than double-stranded DNA (ds26) generally. Moreover, both single-stranded DNA and ribosomal RNA exhibited very weak interaction signal under the same titration conditions. By comparing the terminal functional groups and their positions attached in ligands **1-4**, it seems that ligand **3** possessing a methoxyl group at the *meta*-position of the styryl moiety offers the best discrimination ability towards various nucleic acids. The fluorescence signal induced from the **3**-telo21 complex is about 4-fold higher than that of **3**-ds26 complex. The analogue ligand **4** with two methoxyl groups substituted at *para*- and *meta*-positions gave the worst discrimination ability.
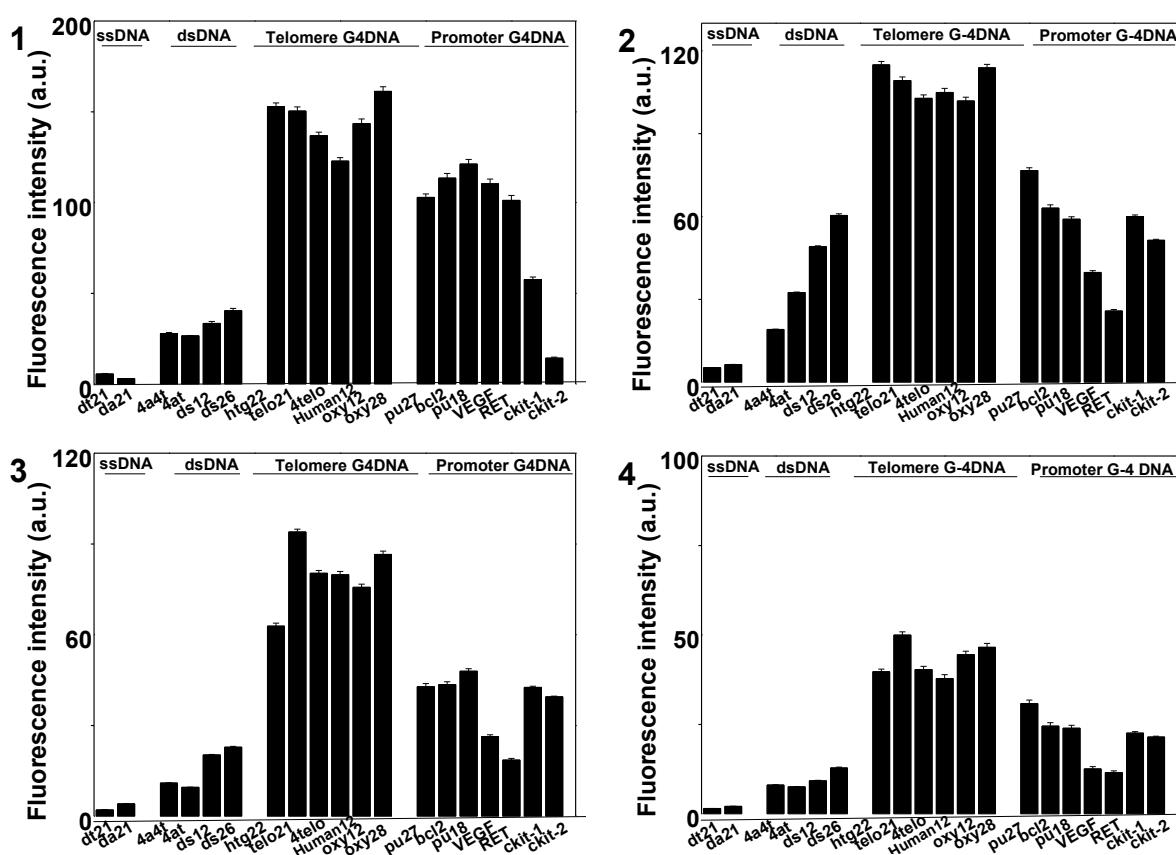
Figure 2. The comparison of substrate selectivity of the binding ligands **1-4** towards various nucleic acids in Tris-HCl buffer solution containing 60 mM KCl. The final concentration of the binding ligand was fixed at 5 μM, and DNA concentration used was 10 μM. For ligand **1** and **4** the excitation wavelength (λ_{ex}) was 475 nm and the emission signal (λ_{em}) was recorded at 530 nm. For ligand **2** and **3** the excitation wavelength (λ_{ex}) was 520 nm and the emission signal (λ_{em}) was recorded at 610 nm. Measurements were taken after incubated for 10 min at room temperature.
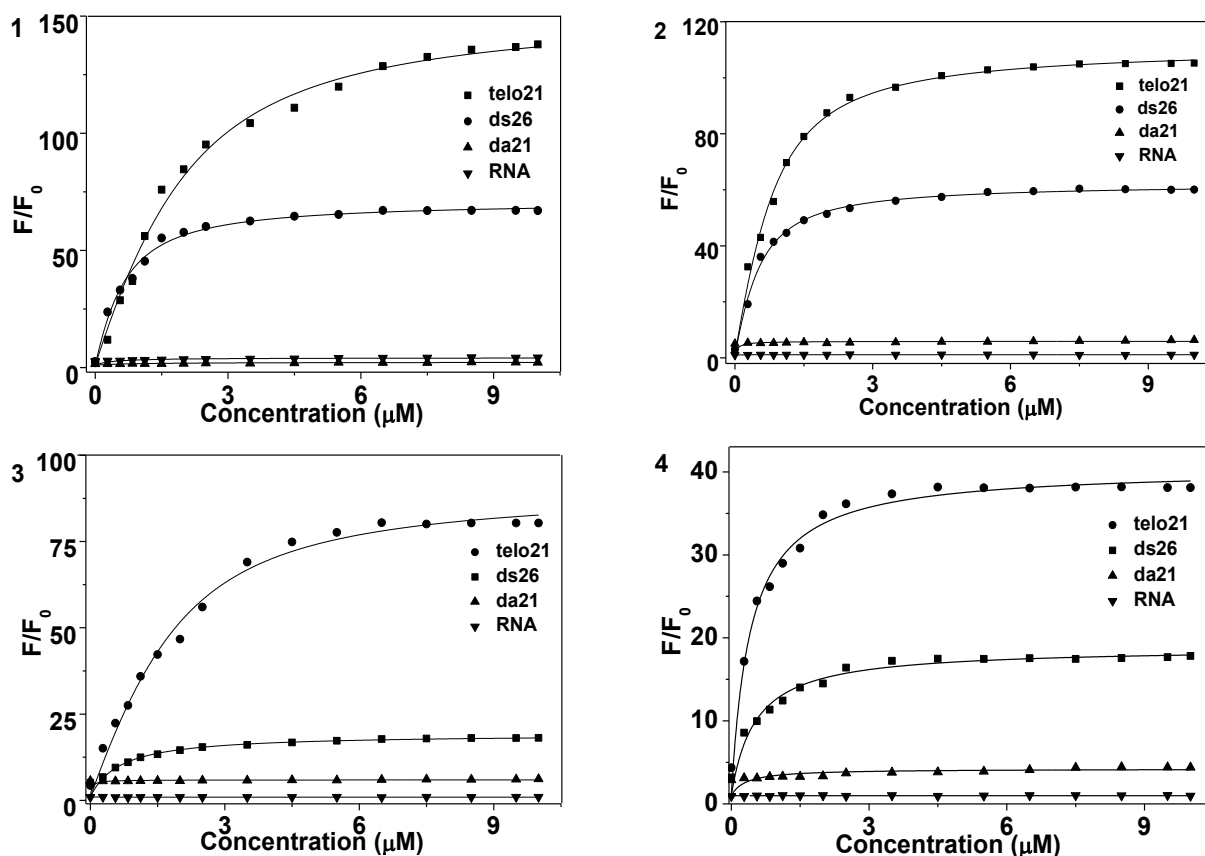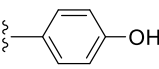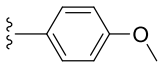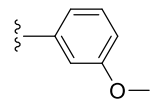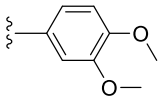
Figure 3. The binding study of ligands **1-4** with various concentration of nucleic acids including single-stranded DNA: da21, double-stranded DNA: ds26, G4-DNA: telo21, and RNA. In the fluorescence titrations (**1, 4**: λ_{ex} = 475 nm, λ_{em} = 530 nm and ligand **2, 3**: λ_{ex} = 520 nm, λ_{em} = 610 nm), the final concentration of ligand was fixed at 5 μM in a Tris–HCl buffer containing 60 mM KCl. Measurements were taken after incubated for 10 min at 25 °C.

From the fluorescence titration experiments, some nucleic acids did not induce the fluorescence binding signals. However, both telo21 (G4-DNA) and ds26 (double stranded DNA) offered significant fluorescence signals for the interaction. The detectable quantum yields of the ligand-telo21 complex were obtained in the range of 0.03-0.14. The equilibrium binding constants of the ligands with telo21 and ds26 were estimated and summarized in Table 1. For nucleic acids of da21 and RNA, the equilibrium binding constants were not able to determine due to their weak binding signal induced in the fluorescence titration assays (Figure 3). In the ligand series, the K_{telo21} values were found in the range of 0.4 - 8.2 x 10^5 M^{-1} while the K_{ds26} were generally weaker (0.3 - 4.5 x 10^5 M^{-1}). This indicated that ligands have higher binding selectivity towards G4-DNA compared to double-stranded DNA. The result seems in accord with the

8

observations obtained in the fluorescent screening of substrates as shown in Figure 2. However, binding constants and fluorescence responses may not necessary have direct relationship for small molecules recognizing nucleic acids.[43,44] Among the four ligands bearing the terminal groups at different positions, **1** has the largest equilibrium binding constants for both telo21 and ds26 probably due to its terminal hydroxyl group at the *para*-position of the styryl moiety contributed to the hydrogen bond interaction with nucleic acid substrates. When this hydroxyl group was changed to methoxyl (**2**), the equilibrium binding constants were dropped obviously (K_{telo21} = 1.9 x 10^5 M^{-1}; K_{ds26} = 1.3 x 10^5 M^{-1}). This result supported that hydroxyl group significantly involved in the ligand-DNA interaction. However, the interaction from hydrogen bonding seems not beneficial to the molecular discrimination towards the DNA structures of telo21 and ds26 as indicated by the K_{telo21}/K_{ds26} ratio, which is just about 1.8 folds. Interestingly, for ligand **3** that has a methoxyl group at the *meta*-position of the styryl moiety, its K_{telo21} (5.6 x 10^5 M^{-1}) is almost 3-fold as high as ligand **2**. The results suggested that the position of the methoxyl group at the terminal styryl moiety is also a critical factor affecting the ligand-DNA interaction with the binding pocket of G-quartet. This result could be further elaborated that the binding pocket of G-quartet may have certain well-defined geometry and spatial constraints; however, the related information is very limited in literature. In addition, the ability of **3** to discriminate G4- and double-stranded DNA is found to be the best, K_{telo21}/K_{ds26} = 3 approximately. Based on the results from the binding study with ligands **1-4**, the linear relationship for fluorescence sensing of telo21 G4-DNA *in vitro* was able to establish as shown in Figure S2. In addition, the molecular interaction between **3** and telo21 was also supported from the UV-vis titration experiments shown in Figure S4. The major absorption peak of ligands **1**-**3** at 506-527 nm were found increased gradually with the addition of telo21. However, ligand **4** showed very weak absorption signal changes.

Table 1. Quantum yields of the ligand-DNA complexes and their equilibrium binding constants.

Ligand	Terminal side-group	Complex Φ_f [b]	K_{telo21} ($\times 10^5$ M^{-1})[c]	K_{ds26} ($\times 10^5$ M^{-1})[d]
1	phenyl–OH	0.05	8.2	4.5
2	phenyl–O–CH₃ (para-methoxy)	0.14	1.9	1.3
3	phenyl–O— (meta)	0.07	5.6	1.8
4	phenyl with –O and O— (dimethoxy)	0.03	0.4	0.3

[a] Experiments were performed in 10 mM Tris-HCl buffer at pH 7.4 at 25 °C.

[b] Relative fluorescence quantum yield of probes upon addition of 3 µM telo21; the standard of the relative fluorescence quantum yield use is fluorescein ($\Phi_f = 0.85$, in 1 % NaOH).

[c] Equilibrium binding constant (K_{telo21}) between the ligand and telo21 G4-DNA.

[d] Equilibrium binding constant (K_{ds26}) between the ligand and ds26 double stranded DNA.

When the ligands titrated with telo21, a strong emission signal was induced evidently and this signal indicates that the ligand-telo21 adduct is formed *in vitro*. The enhanced fluorescence signal may also reveal that the molecular rotating ability (intramolecular torsional motion) of both the benzothiazole group and the terminal phenyl group may be effectively restricted because the molecular size of the ligands are small enough to fit into the G4-binding pocket. Therefore, the favorable adduct may probably form through the intermolecular π-π stacking interactions between the ligand and G4-structure. To predict the possible binding orientations for the ligands in the G4-DNA binding pocket, molecular docking studies were performed for the ligands using an anti-parallel telo21 G-quadruplex structure (PDBID: 2mb3)[45] based on 1 to 1 stoichiometry. All ligands are found binding to the 5' end of the G-quartet via π-π stacking interaction. As shown in Figure 4, the binding modes for ligands **1-4** are very similar. It is noteworthy that the positively charged 1-methylpyridinium moiety is positioned close to the negatively charged carbonyl channel of G-quartet and three aromatic rings (benzothiazole group, benzene ring of

1-methylquinolinium, and the terminal phenyl group) stack on top of three guanine bases of G-quartet to maximize π-π stacking interactions. Ligand **1** with a terminal phenol group has an estimated binding free energy of -8.3 Kcal/mol and is very close to that of its two mono-methoxylated analogues (-8.5 Kcal/mol for **2**; -8.6 Kcal/mol for **3**). The estimated binding free energy for the di-methoxylated analogue **4** is found to be -8.3 Kcal/mol. The docking study of the molecules with telo21 G4-DNA shows very comparable binding free energy. However, the terminal groups of **1** (-OH at *para*-position of the phenyl ring)**, 2** (-OCH$_3$ at *para*-position of the phenyl ring) and **4** (-OCH$_3$ at *para*-position of the phenyl ring) were found located outside the G-tetrad, whereas ligand **3** with its terminal -OCH$_3$ group at *para*-position of the phenyl ring is stacked on the G-tetrad (Figure 4). This may probably maximize the molecular interaction with the G4-binding pocket and give a better fluorescence discrimination signal.
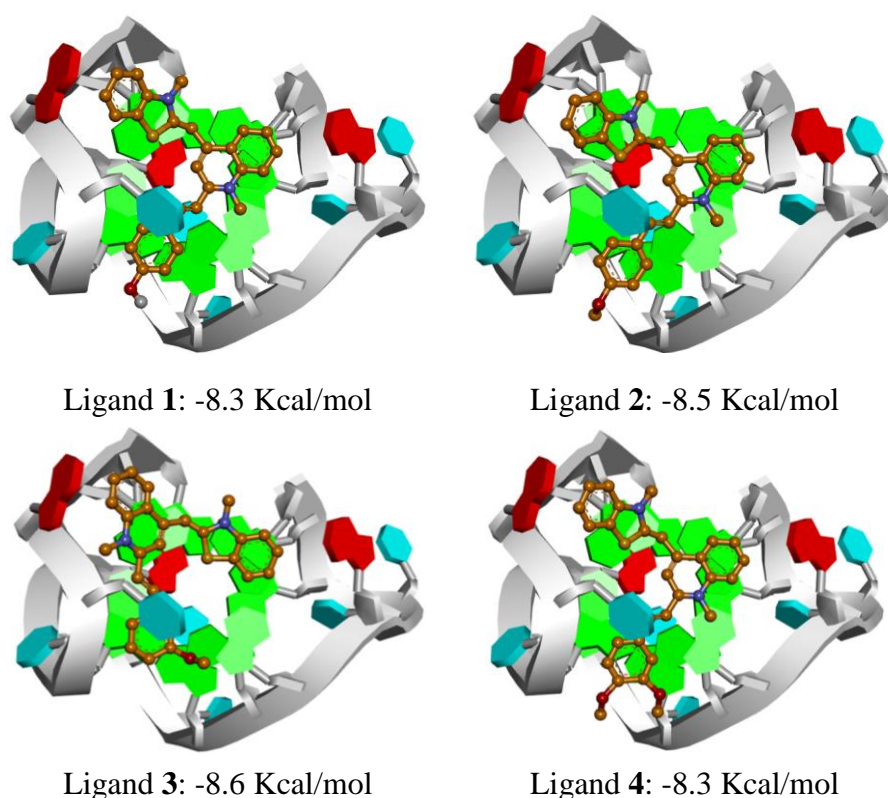

| Ligand **1**: -8.3 Kcal/mol | Ligand **2**: -8.5 Kcal/mol |
| Ligand **3**: -8.6 Kcal/mol | Ligand **4**: -8.3 Kcal/mol |

Figure 4. The binding mode and binding energy of the ligands with telo21 G4-DNA (PDB ID: 2mb3) from molecular docking study based on 1:1 stoichiometry.
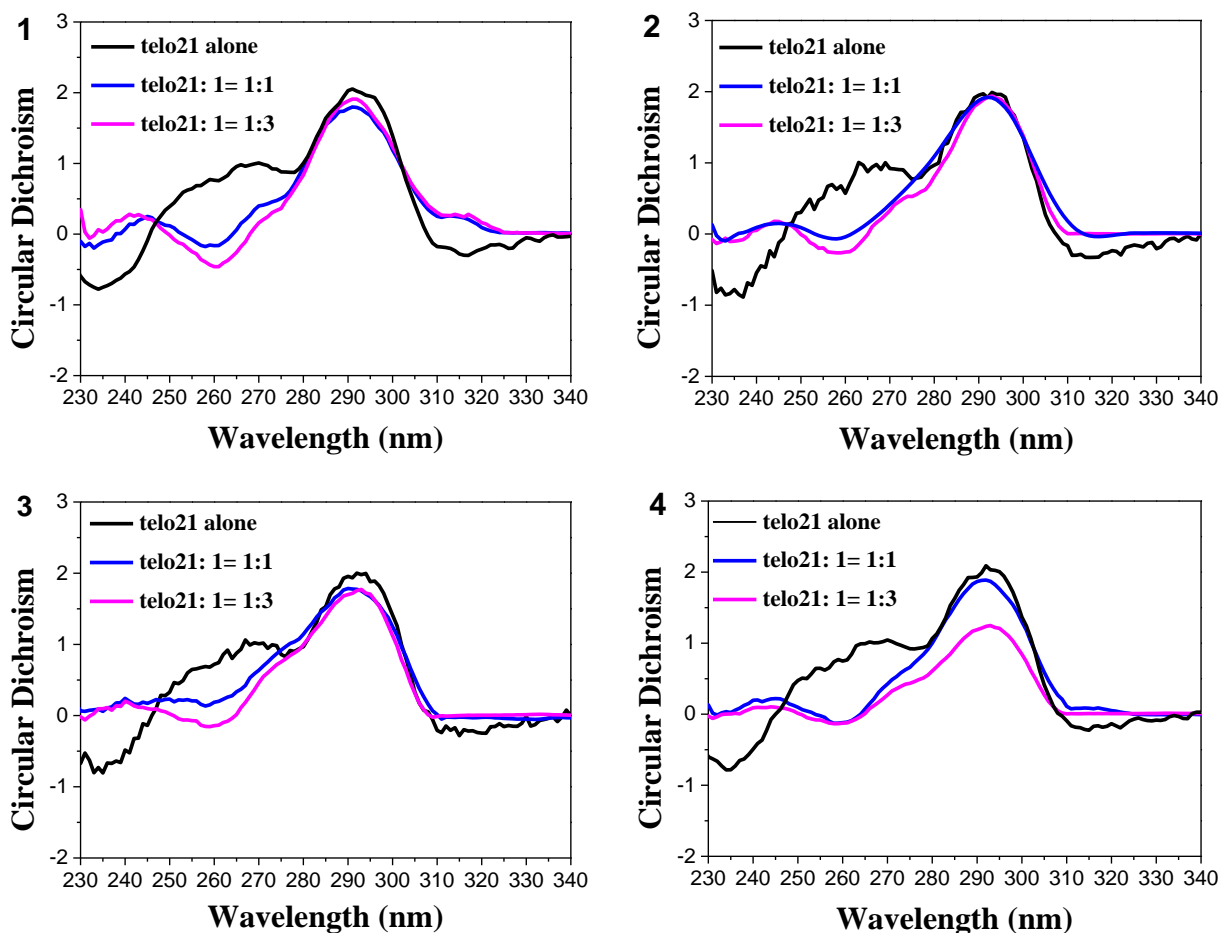
Figure 5. CD spectra of the binding ligands **1-4** bound to telo21 (5 µM) in 10 mM Tris–HCl, 60 mM KCl, pH = 7.4.

To study the possible G4-DNA conformation changes induced by the ligands, circular dichroism (CD) spectroscopy was carried out using telo21 as a model substrate. From the results shown in Figure 5, the CD spectra of telo21 alone showed a major negative absorption band at 235 nm and another two positive bands located at 265 nm and 290 nm, respectively. The absorption pattern may indicate that both parallel and anti-parallel types of topology could co-exist in solution with potassium ions. When adding the ligands to the solution to interact with telo21, the negative absorption band at 235 nm was influenced. The absorption was increased from negative to about zero. A new and weak positive absorption band between 240-245 nm was observed. In addition, as the concentration of ligands increased further, the positive broad absorption bands at 265 nm decreased significantly and became slightly negative. The CD signal changes may indicate that the ligands could possibly influence the topology telo21 upon

interaction. It seems that the parallel-type telo21 G4-structure, which has a typical CD absorption spectrum showing a negative band at 235 nm and a positive band at 265 nm approximately, is significantly influenced. On the contrary, the characteristic positive band at 290 nm and negative band at 265 nm for anti-parallel topology of telo21 were clear observed. This may indicate that telo21 G4-DNA in anti-parallel form has no significant influence upon binding to ligands. The CD results indicate that the ligands could affect parallel topology of telo21 and induce them to fold into anti-parallel, which may probably form a more stable adduct.
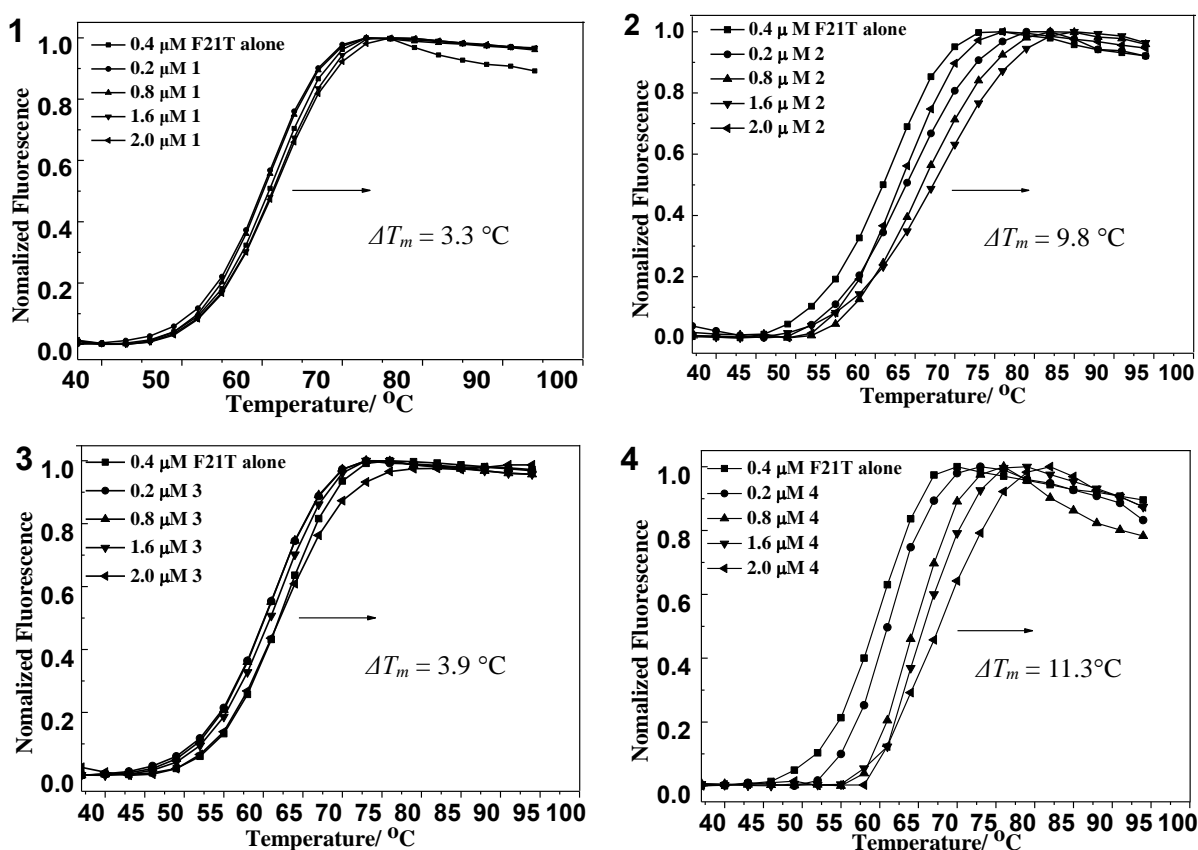
Figure 6. Normalized FRET melting curves of G-quadruplex F21T (0.4 μM) with the addition of different concentration of binding ligands **1-4** (0.2–2.0 μM) in 10 mM Tris–HCl, 60 mM KCl, pH = 7.4.

To compare the stabilization ability of the ligands for the G4-DNA structure, fluorescence resonance energy transfer (FRET) measurements were performed. The normalized FRET melting curves of G-quadruplex F21T DNA at different concentration of ligands were shown in Figure 6. In general, with the ligand concentration at 2 μM, the increased ΔT_m values were observed with a

range from 3.3 to 11.3 °C. These results may suggest that the ligands are able to stabilize the G-quadruplex structure. The control experiments with double-stranded F10T DNA were also examined and the ΔT_m values were about 0.4 to 1.3 °C under the same conditions (Figure S5). It was found that the ligand with the terminal function group of methoxybenzene showed slight better G4-stabilization ability than phenol.

The results of molecular docking study, equilibrium binding constants, and ΔT_m values suggested a favorable and stable interaction of the ligands with G4-structures. We thus examined their cytotoxicity against two cancer cell lines to evaluate the potential of these ligands in anticancer application.[46,47] The cytotoxicity of ligands were studied with MTT assays. Two cell lines including PC3 (human prostate cancer cell) and hepG2 (human hepatoma cell) were selected to examine the inhibitory effect of the ligands on cancer cell growth. From the results listed in Table 2, the ligands showed relatively high cytotoxicity to both types of cancer cells. The IC_{50} values obtained in PC3 and hepG2 cancer cells were in the range of 3.4–10.8 µM. The cytotoxicity observed could be due to the interaction of the ligands with DNAs such as G-quadruplex DNA and/or double stranded DNA *in vivo* to interfere the cell growth,[48] but more in-depth investigations are required to fully understand the underlying mechanism.

Table 2. IC_{50} of ligands evaluated with MTT cytotoxicity assay.[a]

Ligand	IC_{50} (µM)	
	PC3	hepG2
1	6.6	5.8
2	5.6	3.4
3	4.6	6.3
4	10.8	7.5

[a] Inhibition rate (%) = (Control group average OD - Experimental group average OD)/Control group average OD x 100%. $lgIC_{50} = X_m-I (P-(3-P_m-P_n)/4)$. Where X_m: lg(maximum dose); I: lg(maximum dose/adjacent dose); P is the sum of positive response rates; P_m is the largest positive response rate; P_n is the smallest positive response rate.

Conclusion

In conclusion, a number of new fluorescent nucleic acid binding ligands, which possess a terminal functional group of phenol or methoxybenzene, were synthesized to understand their functional difference in the signal of interaction, selectivity, binding affinity and ligand-G4-DNA complex stabilization with a variety of nucleic acids including single-strand DNA, double-stranded DNA, telomere and promoter G4-DNA, and ribosomal RNA. It was found that the position of the terminal methoxyl group showed strong influence on the binding affinity and fluorescence discrimination for G4-DNA against other nucleic acid structures. The results suggested that ligand **3** with a methoxyl group substituted at the *meta*-position of the styryl moiety exhibited the best fluorescence discrimination ability towards G4-DNA against double stranded DNA. The delta T_m obtained from the FRET measurements suggested that the DNA binding ligand with the terminal methoxybenzene group is able to stabilize G4-structures. Moreover, the cytotoxicity of the ligands was examined in PC3 and hepG2 cancer cells. The IC_{50} values obtained were in the range of 3.4–10.8 μM.

Experimental Section

Materials and instrumentation

All chemicals were purchased from commercial sources unless otherwise specified. All the solvents were of analytical reagent grade and were used without further purification. All oligonucleotides used in this work were synthesized and purified by Shanghai Sangon Biotechnology Co. Ltd. (Shanghai, China). Their sequences were given in Table S1. Fluorescence studies were performed on a LS45 luminescence spectrophotometer (Perkin-Elmer, USA). A quartz cuvette with 2 mm x 2 mm path length was used for the spectra recorded at 10 nm slit width for both excitation and emission unless otherwise specified. Mass spectra (MS) were recorded on Bruker amaZon SL mass spectrometer with an ESI or ACPI mass selective detector. ^{1}H and ^{13}C NMR spectra were recorded using TMS as the internal standard in CDCl$_3$ or DMSO-*d$_6$* with a Bruker BioSpin GmbH spectrometer at 400 MHz and 100 MHz, respectively.

The purities of synthesized compounds were confirmed by using analytical HPLC with a dual pump Shimadzu LC-20A system equipped with a photo-diode array detector and a C18 column (250 mm x 4.6 mm, 5 µM YMC) and eluted with acetonitrile/water (47:53) containing 0.5 % acetic acid at a flow rate of 1.0 mL/min. The stock solutions of the ligands were prepared at 5 mM with DMSO. The stock solution was then diluted to the required concentration with Tris–HCl buffer containing 60 mM KCl for experiments.

Fluorescence binding assays

In the fluorescence titration experiments, the excitation wavelength (λ_{ex}) and emission wavelength (λ_{em}) for **1**: λ_{ex} = 475 nm and λ_{em} = 530 nm, for **2**: λ_{ex} = 520 nm and λ_{em} = 610 nm, for **3**: λ_{ex} = 520 nm and λ_{em} = 610 nm, and for **4**: λ_{ex} = 475 nm and λ_{em} = 530 nm were applied. For the titrations, the final concentration of the binding ligand used was fixed at 5 µM in a Tris–HCl buffer containing 60 mM KCl. Measurements were taken after incubated for 10 min at 25 °C. With the data obtained through fluorimetric titrations, the binding constants were analyzed according to the independent site model[49] by nonlinear fitting to the equation[50]: F/F_0 = $1+(Q-1)/2\{A+1+x-[(x+1+A)^2-4x]^{1/2}\}$, where F_0 is the fluorescence intensity of **1**–**4** in the absence of DNA, F_{max} is the fluorescence intensity upon saturation of DNA, $Q = F_{max}(F_0)^{-1}$, $A = (K_{eq}C_{dye})^{-1}$, and $x = nC_{DNA}(C_{dye})^{-1}$; n is the putative number of binding sites on a given DNA matrix. The parameters Q and A were found via the Levenberg−Marquardt fitting routine in the Origin 8.5 software, whereas n was varied to obtain the best fit. The calculated binding stoichiometry of ligands **1-4** with G-quadruplex telo21 was listed in Table S2 in supporting information.

The limit of detection was calculated on the basis of the equation: LOD = n × S_b/m; n value in accordance with the International Union of Pure and Applied Chemistry (IUPAC) is generally taken to be 3; S_b represents the standard deviation of the blank multiple measurements (n = 20); m is the slope of the calibration curve representing the sensitivity of this method.[51]

Fluorescent quantum yields

The fluorescent quantum yields of the binding ligands in the presence of DNA were calculated

using fluorescein in 1 % NaOH ethanol as standard (Φ = 0.85).[52] Absorbance and fluorescence values were recorded after adding five solutions with an increasing concentration of a selected sample into fixed a concentration of DNA solution. Quantum yields were calculated according to the equation[53]: $\Phi_x = \Phi_{ST} (Grad_x / Grad_{ST}) (\eta^2_x / \eta^2_{ST})$; where the subscripts ST and X denote the standard and test respectively; Φ is the fluorescence quantum yield; Grad is the gradient from the plot of integrated fluorescence intensity versus absorbance, and is the refractive index of the solvent.

Molecular docking study

Molecular docking study was performed using the solution structure of anti-parallel human telomeric DNA G-quadruplex (PDBID: 2mb3)[45]. The first two thymine residues at the 5' end and the last residue adenine at the 3' end were deleted to produce 21-mer G-quadruplex. The 3D structures of the small molecules were generated with DS viewer 3.5. Autodock Tools (ver. 1.5.6) was used to convert the structure files to pdbqt format.[54] Docking was performed using the AUTODOCK vina program.[55] The dimensions of the active site box were chosen to be large enough to encompass the entire G-quadruplex structures. An exhaustiveness of 20 was used and other parameters were left as default.

Circular dichroism (CD) measurement

The concentration of telo21 was 5 μM in 10 mM Tris−HCl, 60 mM KCl, pH = 7.4, and the concentration of conjugate was 1 to 4 folds in 5 mM Tris-HCl with 60 mM KCl at pH 7.4. The CD spectra were carried out using a Chirascan spectrophotometer (Applied Photophysics). The quartz cuvette with 4 mm path length was employed for the spectra recorded over a wavelength range of 230 to 450 nm at 1 nm bandwidth, 1 nm step size, and 0.5 s per point. The CD spectra were obtained by taking the average of at least three scans made from 230 to 450 nm at 25 °C. Final analysis of the data was carried out with Origin 7.5 (OriginLab Corp.).

FRET assay conditions

The FRET assay was performed as a high-throughput screen following previously published

procedures.27 The labeled oligonucleotides F21T: 5'-FAM-d(GGG[TTAGGG]3)-TAMRA-3' (donor fluorophore FAM is 6-carboxyfluorescein; acceptor fluorophore TAMRA is 6-carboxytetramethylrhodamine; HEG linker is ($-CH_2-CH_2-O-$)$_6$ used as the FRET probes were diluted from stock to the correct concentration (0.4 μM) in buffer and then annealed by heating to 95 °C for 5 min, followed by cooling to room temperature. Samples were prepared by aliquoting 15 μL of the annealed F21T (at 2 × concentration, 0.4 μM) into LightCycler 96, followed by 15 μL of the ligand solution (at 2 × concentration, 0.2–2.0 μM) and further incubated for 1 h. Fluorescence melting curves were determined with a Roche LightCycler real-time PCR machine with excitation at 470 nm and detection at 530 nm. Fluorescence readings were taken at intervals of 3 °C over the range 37–93 °C, with a constant temperature being maintained for 300 s prior to each reading to ensure a stable value.

MTT experiment conditions

The cell lines at logarithmic growth stage were inoculated into two 96-well plates with a cell density of about 5000 cells per hole and then exposed to 37 °C and 5 % CO_2 respectively. After 48 h of inoculation, the medium was discarded, washed three times with PBS buffer, and then added to the medium containing different concentrations of gradient compounds. After incubation for 48 h, MTT (thiazole blue) solution (5 mg/mL) 20 μL was added into each hole (blank group without MTT coloration and control group without medicine). Continue incubation for 4 h at 37 C and 5% CO_2, the supernatant was discarded and DMSO 100 μL was added into each hole. After 15 s of oscillation, the chlamydia was fully dissolved. Finally, the absorbance of each hole at 492 nm was measured by enzyme labeling instrument, and the experimental results were recorded. The IC_{50} value of the compound can be obtained by mapping the cell viability.

General procedures for the synthesis of DNA-binding ligands 1–4

The starting compound, (Z)-1,2-dimethyl-4-((3-methylbenzo[d]thiazol-2(3H)-ylidene)methyl)quinolin-1-ium iodide, was synthesized according to the reported procedures.[56] The compound (0.16 mmol) and 4-methylpiperidine (0.5 mL) were well-mixed in a flask containing 10 ml n-butanol at room

temperature. To this solution a suitable aromatic aldehyde (0.32 mmol) was added. The reaction mixture then was refluxed for 3 h. After that, the reaction mixture was cooled in an iced-bath and the precipitates were formed. The precipitates were then filtered by suction filtration. The collected solids were washed with *n*-butanol at room temperature. The precipitate collected was further purified with flash column chromatography to afford the pure compounds **1−4**. All these compounds were fully characterized with ^{1}H & ^{13}C NMR, ESI-MS, HPLC before using for measurements and bioassays. The characterizations of each compound were listed as follows:

For ligand **1**, the deep violet solid was isolated with 88 % yield. The melting point was 275-281°C; ^{1}H NMR (400 MHz, DMSO) δ 8.61 (d, *J* = 8 Hz, 1H), 7.98 (t, *J* = 8 Hz, 2H), 7.87 (t, *J* = 8 Hz,1H), 7.75 (d, *J* = 8 Hz, 2H), 7.64 (t, *J* = 8 Hz, 1H), 7.52-7.46 (m, 3H), 7.45-7.31 (m, 3H), 6.87 (d, J = 8 Hz, 2H), 6.68 (s, 1H), 4.01 (s, 3H), 3.83 (s, 3H). ^{13}C NMR (100 MHz, DMSO) δ 160.39, 159.11, 152.57, 147.55, 141.65, 140.78, 139.26, 133.45, 131.04, 128.37, 126.71, 125.49, 124.38, 124.09, 123.73, 123.32, 118.79, 117.93, 116.25, 112.79, 107.92, 87.81, 38.36, 33.99. ESI-MS for [M–I]$^+$ ($C_{27}H_{23}N_2OS^+$): m/z 423.1; HPLC retention time with an eluent CH_3CN: 0.5 % $CH_3COOH_{(aq)}$ = 53:47 (v/v) was 2.18 min. The purity of the compound was higher than 95%.

For ligand **2**, the dark brown solid was isolated with 84 % yield. The melting point was 263-267 °C; ^{1}H NMR (400 MHz, DMSO) δ 8.73 (d, *J* = 8.4 Hz, 1H), 8.10 (d, *J* = 8.4 Hz, 1H), 8.06 (d, *J* = 7.6 Hz, 1H), 7.96 (t, *J* = 7.6 Hz, 1H), 7.92 (d, *J* = 8.4 Hz, 2H), 7.73 (t, *J* = 7.6 Hz, 1H), 7.66 (d, *J* = 8.4 Hz, 1H), 7.60 (m, 3H), 7.51 (s, 1H), 7.40 (t, *J* = 7.6 Hz, 1H), 7.09 (d, *J* = 8.4 Hz, 2H), 6.82 (s, 1H), 4.11 (s, 3H), 3.96 (s, 3H), 3.91 (s, 3H). ^{13}C NMR (100 MHz, DMSO) δ 160.41, 158.29, 151.39, 146.68, 140.01, 139.75, 138.21, 132.41, 129.64, 127.29, 127.12, 125.65, 124.43, 123.36, 123.04, 122.70, 122.25, 118.06, 117.75, 113.67, 111.81, 106.95, 86.87, 54.80, 37.30, 32.91. ESI-MS for [M–I]$^+$ ($C_{28}H_{25}N_2OS^+$): m/z 437.0; HPLC retention time with an eluent CH_3CN: 0.5 % $CH_3COOH_{(aq)}$ = 53:47 (v/v) was 2.95 min. The purity of the compound was higher than 95%.

For ligand **3**, the reddish brown solid was isolated with 81 % yield. The melting point was 252-256 °C; ^{1}H NMR (400 MHz, DMSO) δ 8.50 (d, *J* = 8.5 Hz, 1H), 7.78 (m, 3H), 7.70 (d, *J* = 8.0 Hz, 1H), 7.57 (m, 2H), 7.39 (m, 3H), 7.31 (d, *J* = 8.0 Hz, 1H), 7.24 (t, *J* = 7.2 Hz, 1H), 7.09 (s,

1H), 6.99 (t, J = 7.2 Hz, 1H), 6.92 (d, J = 8.5 Hz, 1H), 6.52 (s, 1H), 3.83 (s, 3H), 3.74 (s, 3H), 3.65 (s, 3H). ^{13}C NMR (100 MHz, DMSO) δ 158.57, 157.74, 152.11, 147.18, 140.32, 138.85, 135.87, 133.43, 132.33, 128.64, 128.40, 126.69, 125.29, 124.49, 123.62, 123.54, 123.47, 122.65, 121.28, 121.09, 118.61, 112.79, 111.99, 107.86, 87.84, 56.28, 38.22, 34.02. ESI-MS: [M–I]$^+$ ($C_{28}H_{25}N_2OS^+$): m/z 437.0; HPLC retention time with an eluent CH_3CN/ 0.5 % $CH_3COOH_{(aq)}$ = 53:47 (v/v) was 3.14 min. The purity of the compound was higher than 95%.

For ligand **4**, the deep reddish brown solid was isolated with 89 % yield. The melting point was 266-270 °C; ^{1}H NMR (400 MHz, DMSO) δ 8.73 (d, J = 12 Hz, 1H), 8.16 (d, J = 8 Hz, 1H), 8.05 (d, J = 8 Hz, 1H), 8.05-7.80 (m, 2H), 7.69 (s, 1H), 7.65-7.52 (m, 3H), 7.52-7.35 (m, 3H), 7.07 (d, J = 8 Hz, 1H), 6.85 (s, 1H), 6.70-6.6 (m, 1H), 4.16 (s, 3H), 3.97 (s, 3H), 3.91 (s, 3H), 3.85 (s, 3H). ^{13}C NMR (100 MHz, DMSO) δ 158.57, 157.74, 152.11, 147.13, 140.32, 138.85, 135.87, 133.43, 132.33, 128.64, 128.40, 126.69, 125.29, 124.49, 123.62, 123.54, 123.47, 122.65, 122.41, 87.70, 56.28, 37.96, 33.94. [M–I]$^+$ ($C_{29}H_{27}N_2O_2S^+$): m/z 467.0; HPLC retention time with an eluent CH_3CN: 0.5 % $CH_3COOH_{(aq)}$ = 53:47 (v/v) was 5.72 min. The purity of the compound was higher than 95%.

Acknowledgement

Reference

[1] R. Y. Tsien, *Annu. Rev. Neurosci.*, **1989**, *12*, 227-253.

[2] M. J. Lohse, S. Nuber, C. Hoffmann, *Pharmacol. Rev.*, **2012**, *64*, 299-336.

[3] A. T. Aron, K. M. Ramos-Torres, J. A. Cotruvo Jr, C. J. Chang, *Acc. Chem. Res.*, **2015**, *48*, 2434-2442.

[4] M. C. Heffern, H. M. Park, H. Y. Au-Yeung, G. C. V. Bittner, C. M. Ackerman, Andreas Stahl,

C. J. Chang, *P. Natl. Acad. Sci.*, **2016**, *113*, 14219-14224.

[5] J. L. Kolanowski, F. Liu, E. J. New, *Chem. Soc. Rev.*, **2018**, *47*, 195-208.

[6] R. Kumari, D. Sunil, R. S. Ningthoujam, *Bioorg. Chem.*, **2019**, *88*, 102979.

[7] D. J. Stephens, V. J. Allan, *Science*, **2003**, *300*, 82-86.

[8] X. Su, X. J. Xiao, C. Zhang, M. P. Zhao, *Appl. Spectrosc.*, **2012**, *66*, 1249-1261.

[9] A. Shivanandan, H. Deschout, M. Scarselli, A. Radenovic, *FEBS Lett.*, **2014**, 588, 3595-3602.

[10] T. Terai, T. Nagano, *Pflugers Arch*, **2013**, *465*, 347-359.

[11] M. Maekawa, G. D. Fairn, *J. Cell Sci.*, **2014**, *127*, 4801-4812.

[12] X. P. He, H. Tian, *Chem*, **2018**, *4*, 246-268.

[13] V. Talianová, T. Břízaa, L. Krčová, B. Dolenský, J. Králová, P. Martásek, V. Krála, M. Havlík, *Bioorg. Chem.*, **2020**, *94*, 103447.

[14] A. G. Coman, A. Paun, C. C. Popescu, N. D. Hădade, A. Hanganu, G. Chiritoiu, I. C. Farcasanu, M. Matache, *Bioorg. Chem.*, **2019**, *92*, 103295.

[15] J. Zhang, K.-L. Wong, W.-K. Wong, N.-K. Mak, D. W. J. Kwong, H.-L. Tam, *Org. Biomol. Chem.*, **2011**, *9*, 6004- 6010.

[16] Z. Liang, T.-H. Tsoi, C.-F. Chan, L. Dai, Y. Wu, G. Du, L. Zhu, C.-S. Lee, W.-T. Wong, G.-L. Law, K.-L. Wong, *Chem. Sci.*, **2016**, *7*, 2151-2156.

[17] L. Stefan, D. Monchaud, *Nat. Rev. Chem.*, **2019**, *3*, 650–668.

[18] L. Ge, Q. Hong, H. Li, C. Liu, F. Li, *Adv. Funct. Mater.*, **2019**, *29*, 1904000.

[19] A. D. Johnson, R. Zammit, J. Vella, M. Valentino, J. A. Buhagiar, D. C. Magri, *Bioorg. Chem.*, **2019**, *93*, 103287.

[20] Z. Lu, Y. Lu, X. Sun, C. Fan, Z. Long, L. Gao, *Bioorg. Chem.*, **2019**, *92*, 103215.

[21] S. Cox, *Dev. Biol*, **2015**, *401*, 175-181.

[22] S. Ray, J. R. Widom, N. G. Walter, *Chem. Rev.*, **2018**, 118, 4120-4155

[23] A. C. Bhasikuttan, J. Mohanty, *Chem. Commun.*, **2015**, *51*, 7581-7597.

[24] A. Laguerre, K. Hukezalie, P. Winckler, F. Katranji, G. Chanteloup, M. Pirrotta, J. M. Perrier-Cornet, J. M. Y. Wong, D. Monchaud, *J. Am. Chem. Soc.*, **2015**, *137*, 8521-8525.

[25] Y. V. Suseela, N. Narayanaswamy, S. Pratihar, T. Govindaraju, *Chem. Soc. Rev.*, **2018**, *47*, 1098-1131.

[26] J.-W. Yan, W.-J. Ye, S.-B. Chen, W.-B. Wu, J.-Q. Hou, T.-M. Ou, J.-H. Tan, D. Li, L.-Q. Gu, Z.-S. Huang, *Anal. Chem.* **2012**, *84*, 6288−6292.

[27] P. Yang, A. De Cian, M.-P. Teulade-Fichou, J.-L. Mergny, D. Monchaud, *Angew. Chem. Int. Ed.*, **2009**, *48*, 2188 –2191.

[28] R. Kumar, K. Chand, S. Bhowmik, R. N. Das, S. Bhattacharjee, M. Hedenström, E. Chorell, *Nucleic Acids Res.*, **2020**, *48*, 1108-1119.

[29] A. Shivalingam, M. A. Izquierdo, A. L. Marois, A. Vyšniauskas, K. Suhling, M. K. Kuimova, R. Vilar, *Nat. Commun.*, **2015**, *6*, 1-10.

[30] W. Long, Y. J. Lu, K. Zhang, X. H. Huang, J. Hou, S. Y. Cai, Y. Li, X. Du, L. G. Luyt, W. L. Wong, C. Chow, *Dyes Pigment.*, **2018**, *159*, 449-456.

[31] N. Sun, C. Wang, M. H. Xu, Y. J. Lu, Y. Y. Zheng, Y. Yan, X. Guo, J. Hou, K. Zhang, L. G.

Luyt, W. L. Wong, C. Chow, *Sensor. Actuat. B: Chem.*, **2017**, *250*, 543-551.

[32] D. Li, W. Long, J. Hou, Q. Deng, Q. Guo, W. L. Wong, Y. J. Lu, K. Zhang, *J. Lumin.*, **2019**, *205*, 367-373.

[33] Y. J. Lu, D. P. Hu, K. Zhang, W. L. Wong, C. Chow, *Biosen. Bioelectron.*, **2016**, 81, 373-381.

[34] D. Li, J. Hou, W. Long, Y. J. Lu, W. L. Wong, K. Zhang, *RSC Adv.*, **2018**, *8*, 20222-20227.

[35] P. Yang, A. De Cian, M.-P. Teulade-Fichou, J.-L. Mergny, D. Monchaud, *Angew. Chem. Int. Ed.*, **2009**, *48*, 2188-2191.

[36] X. Xie, M. Zuffo, M.-P. Teulade-Fichou, A. Granzhan, *Beilstein J. Org. Chem.*, **2019**, *15*, 1872–1889.

[37] D. Monchaud, arXiv:1910.07023 [q-bio.BM], **2019**.

[38] H. Sato, V. Chuang, K. Yamasaki, N. Yamaotsu, H. Watanabe, K. Nagumo, M. Anraku, D. Kadowaki, Y. Ishima, S. Hirono, M. Otagiri, T. Maruyama, *PLoS ONE*, **2014**, *9*,1-12.

[39] F. Giamogante, I. Marrocco, D. Romaniello, M. Eufemi, S. Chichiarelli, F. Altieri, *Oxid. Med. Cell. Longev.*, **2016**, 5, 1-12.

[40] G. Traversi, M. Fiore, S. Leone, E. Basso, E. D. Muzio, F. Polticelli, F. Degrassi, R. Cozzi, *Mutagenesis*, **2016**, *31*, 433-441.

[41] Y. J. Lu, D. P. Hu, Q. Deng, Z. Y. Wang, B. Huang, Y. X. Fang, K. Zhang, W. L. Wong, *Analyst*, **2015**, *140*, 5998-6004.

[42] G. L. Silva, V. Ediz, D. Yaron, B. A. Armitage, *J. Am. Chem. Soc.*, **2007**, *129*, 5710-5718.

[43] D.-M. Kong, Y.-E. Ma, J.-H. Guo, W. Yang, H.-X. Shen, *Anal. Chem.*, **2009**, *81*, 2678–2684.

[44] J. Mohanty, N. Barooah, V. Dhamodharan, S. Harikrishna, P. I. Pradeepkumar, A. C. Bhasikuttan, *J. Am. Chem. Soc.*, **2013**, *135*, 367-376.

[45] W. J. Chung, B. Heddi, M. Tera, K. Iida, K. Nagasawa, A. T. Phan, *J. Am. Chem. Soc.*, **2013**, *135*, 13495-135012.

[46] J. L. Mergny, C. Helene, *Nat. Med.*, **1998**, *4*, 1366-1367.

[47] S. Balasubramanian, L. H. Hurley, S. Neidle, *Nat. Rev. Drug. Discov.*, **2011**, *10*, 261-275.

[48] J. F. Riou, L. Guittat, P. Mailliet, A. Laoui, E. Renou, O. Petitgenet, F. Mégnin-Chanet, C. Hélène, J. L. Mergny, *Proc Natl Acad Sci.,* **2002**, *99*, 2672-2677.

[49] F. H. Stootman, D. M. Fisher, A. Rodger, J. R. Aldrich-Wright, *Analyst*, **2006**, *131*, 1145-1151.

[50] X. Xie, B. Choi, E. Largy, R. Guillot, A. Granzhan, M. P. Teulade-Fichou, *Chem. Eur. J.,* **2013***, 19*, 1214-1226.

[51] B. Qiu, L. Guo, W. Wang, G. Chen, *Biosens. Bioelectron.* **2007**, 22, 2629-2635.

[52] C. Würth, M. Grabolle, J. Pauli, M. Spieles, *Nature Protocols*, **2013**, *8*, 1535-1550.

[53] H. J. Yvon, A Guide to Recording Fluorescence Quantum Yields, Stanmore, Middlesex, UK, **2012**.

[54] G. Morris, R. Huey, *J. Comput. Chem.*, **2009**, *30*, 2785-2791.

[55] S. Forli, R. Huey, M. E. Pique, M. F. Sanner, D. S. Goodsell, *Nat. Protoc.*, **2016**, *11*, 905–9012.

[56] A. D. Cian, L. Guittat, M. Kaiser, B. Saccà, S. Amrane, A. Bourdoncle, P. Alberti, M. P.

Teulade-Fichou, L. Lacroix, J. L. Mergny, *Methods*, **2007**, *42*, 183-195.

Supporting Information

Synthesis of fluorescent G-quadruplex DNA binding ligands for the comparison of terminal group effects in molecular interaction: phenol versus methoxybenzene

Jingwei Jin[b,d,‡], Jinqiang Hou[c,‡],Wei Long[d], Xinyue Zhang[b], Yu-Jing Lu[d], Dongli Li[b], Kun Zhang[b] and Wing-Leung Wong[a,b*]

[a] The State Key Laboratory of Chemical Biology and Drug Discovery, Department of Applied Biology and Chemical Technology, The Hong Kong Polytechnic University, Hung Hom, Kowloon, Hong Kong, China.
[b] School of Biotechnology and Health Sciences, Wuyi University, Jiangmen 529020, P.R. China; and International Healthcare Innovation Institute (Jiangmen), Jiangmen 529040, P.R. China.
[c] Department of Chemistry, Lakehead University and Thunder Bay Regional Health Research Institute, 980 Oliver Road, Thunder Bay, On, P7B 6V4, Canada.
[d] Institute of Natural Medicine and Green Chemistry, School of Chemical Engineering and Light Industry, Guangdong University of Technology, Guangzhou 510006, P. R. China.

[‡] The authors contributed equally to this work.
* Corresponding author
E-mail: wing.leung.wong@polyu.edu.hk

Table S1. Sequences of oligonucleotides used in the present study

Abbreviation	Sequence (5' to 3')	Structure/origin
da21	AAAAAAAAAAAAAAAAAAAAA	single-stranded
dt21	TTTTTTTTTTTTTTTTTTTTT	single-stranded
4a4t	AAAATTTT	Duplex
4at	ATATATATATAT	Duplex
ds12	GCGCAATTGCGC	Duplex
ds26	CAATCGGATCGAATTCGATCCGATTG	Duplex
htg22	AGGGTTAGGGTTAGGGTTAGGG	Telomere G-quadruplex
oxy28	GGGGTTTTGGGGTTTTGGGGTTTTGGGG	Telomere G-quadruplex
telo21	GGGTTAGGGTTAGGGTTAGGG	Telomere G-quadruplex
bcl2	GGGCGCGGGAGGAAGGGGGCGGG	Promoter G-quadruplex
ckit1	AGGGAGGGCGCTGGGAGGAGGG	Promoter-G-quadruplex
ckit2	GGGCGGGCGCGAGGGAGGGG	Promoter G-quadruplex
pu27	TGGGGAGGGTGGGGAGGGTGGGGAAGG	Promoter G-quadruplex
pu18	AGGGTGGGGAGGGTGGGG	Promoter G-quadruplex
4telo	GGGTTAGGGTTAGGGTTAGGGTTAGGGTTAG	Telomere G-quadruplex
oxy12	GGGGTTTTGGGG	Telomere G-quadruplex
VEGF	GGGGCGGGCCGGGGGCGGGG	promoter G-quadruplex
RET	GGGGCGGGGCGGGGCGGGGG	Promoter G-quadruplex
Human12	TTAGGGTTAGGG	Telomere G-quadruplex
RNA	16S- and 23S-Ribosomal from *E. coli*	Duplex
F21T	FAM-(G_3[TTAGGG]$_3$)-TAMRA	Telomere G-quadruplex
F10T	FAM-TATAGCTA-HEG-TATAGCTATAT-TAMRA	Duplex

Table S2. The binding stoichiometry and other parameter (A, Q) calculated for the fluorimetric titrations with ligands **1-4** and G-quadruplex

Parameters	Ligands			
	1	**2**	**3**	**4**
A	36.24	32.52	19.34	11.04
Q	56.13	47.61	18.62	8.75
n	**0.85**	**0.91**	**1.01**	**0.79**

With the data obtained from fluorimetric titrations, the binding constants were analyzed according to the independent site model by nonlinear fitting to the following equation:

$$F/F_0 = 1+(Q-1)/2\{A+1+x-[(x+1+A)^2-4x]^{1/2}\}$$

Where F_0 is the fluorescence intensity of **1–4** in the absence of DNA;

F_{max} is the fluorescence intensity upon saturation of DNA;

$Q = F_{max}(F_0)^{-1}$;

$A = (K_{eq}C_{dye})^{-1}$ and

$x = nC_{DNA}(C_{dye})^{-1}$;

n is the putative number of binding sites on a given DNA matrix.

The parameters, Q and A, were obtained via the Levenberg−Marquardt fitting routine in the Origin 8.5 software, whereas n was varied to obtain the best fit.

Table S3. IC_{50} of ligands evaluated with MTT cytotoxicity assay.[a]

Ligand	IC_{50} (µM)	
	PC3	hepG2
1	6.6	5.8
2	5.6	3.4
3	4.6	6.3
4	10.8	7.5

[a] Inhibition rate (%) = (Control group average OD - Experimental group average OD)/Control group average OD x 100%. $lgIC_{50} = X_m-I (P-(3-P_m-P_n)/4)$. Where X_m: lg(maximum dose); I: lg(maximum dose/adjacent dose); P is the sum of positive response rates; P_m is the largest positive response rate; P_n is the smallest positive response rate.

Figure S1. UV-vis absorption spectra of the ligands in various solvents and the fluorescent enhancement property of the ligands **1-4** in solution with different concentrations of glycerol.
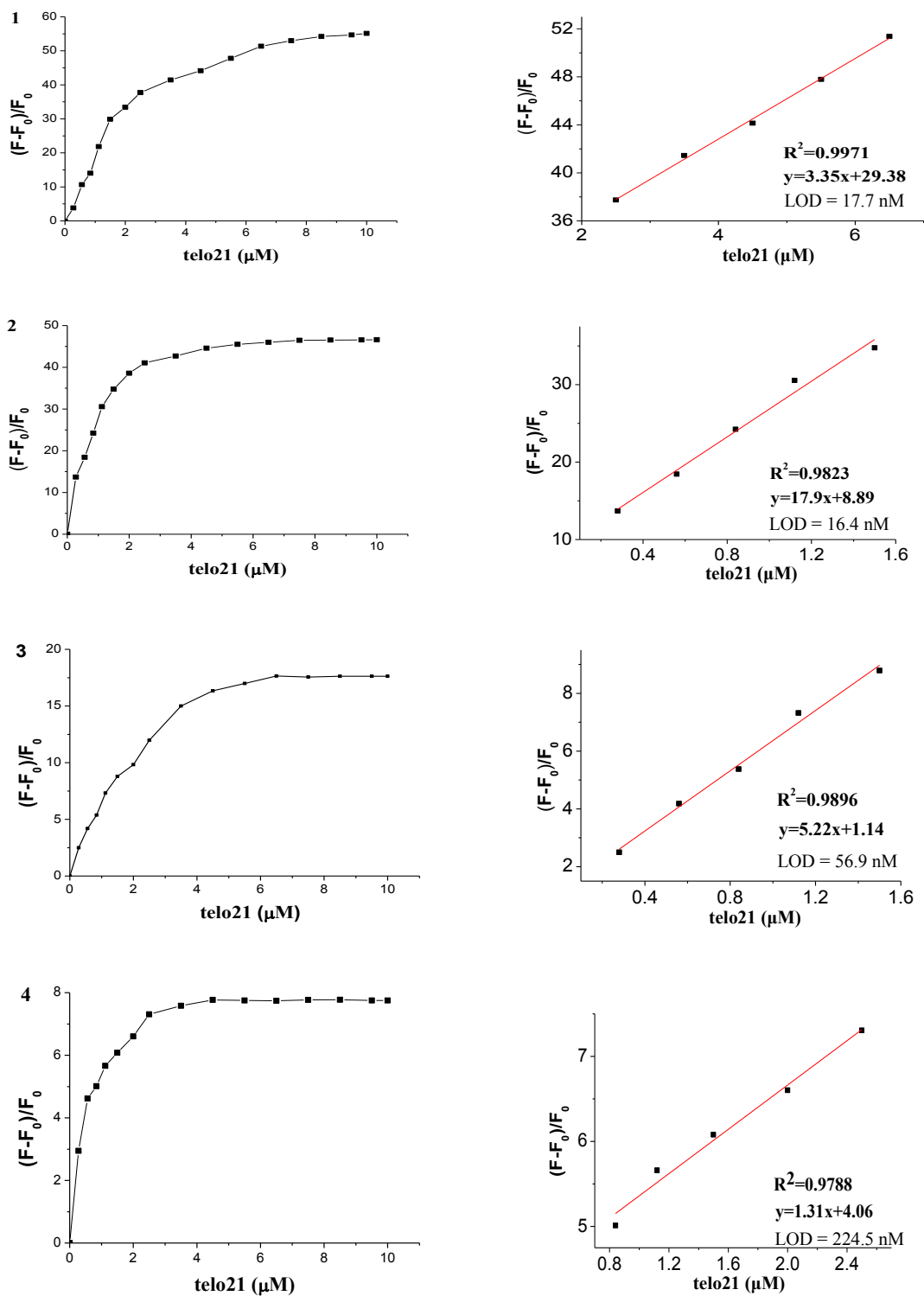
Figure S2. The estimation of linear relationship and LOD for the determination of telo21 binding ligands **1-4**. The final ligand concentration was fixed at 5 μM in a Tris–HCl buffer containing 60 mM KCl at 25 °C.
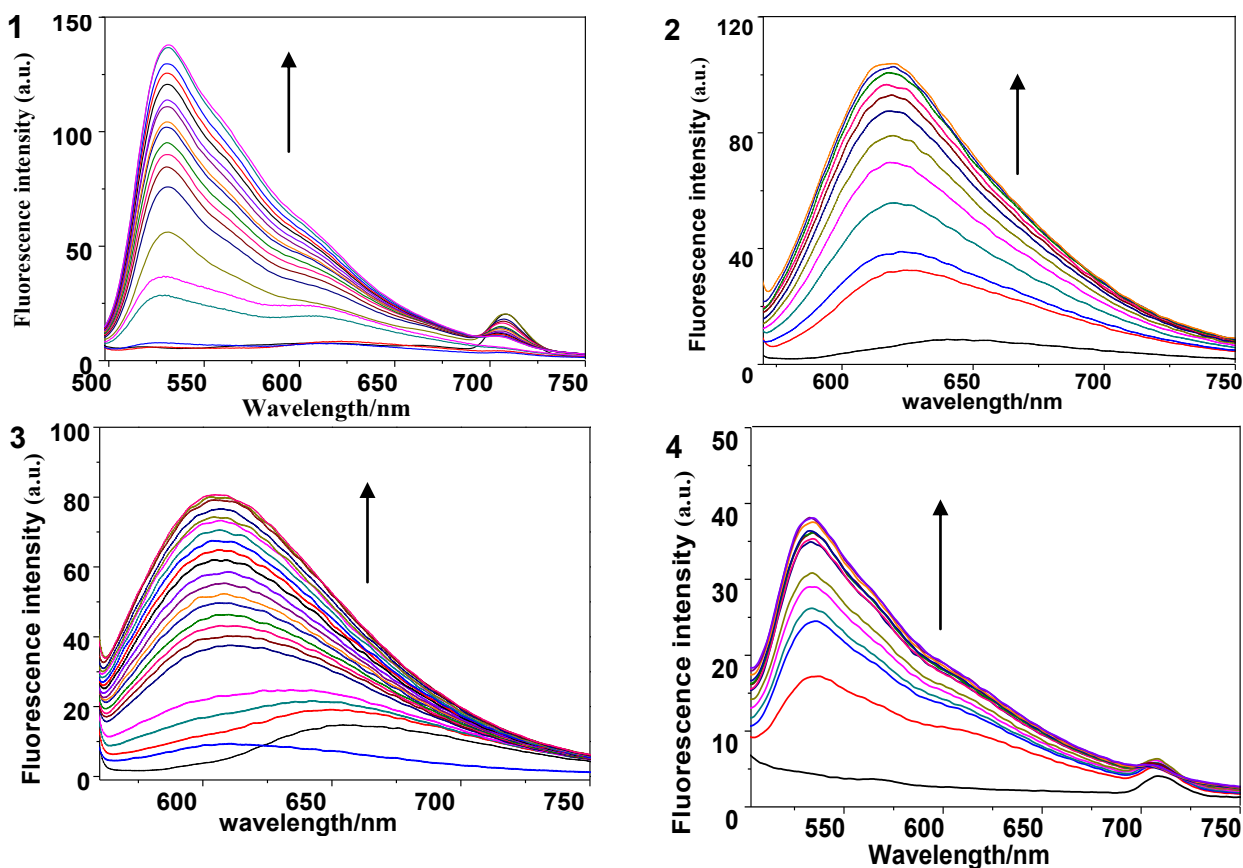
Figure S3. Fluorescence titrations of ligands with telo21 G4-DNA at 25 °C. The final ligand concentration was fixed at 5 μM in a Tris–HCl buffer containing 60 mM KCl. Concentration of telo21 was from 0 to 10 μM.
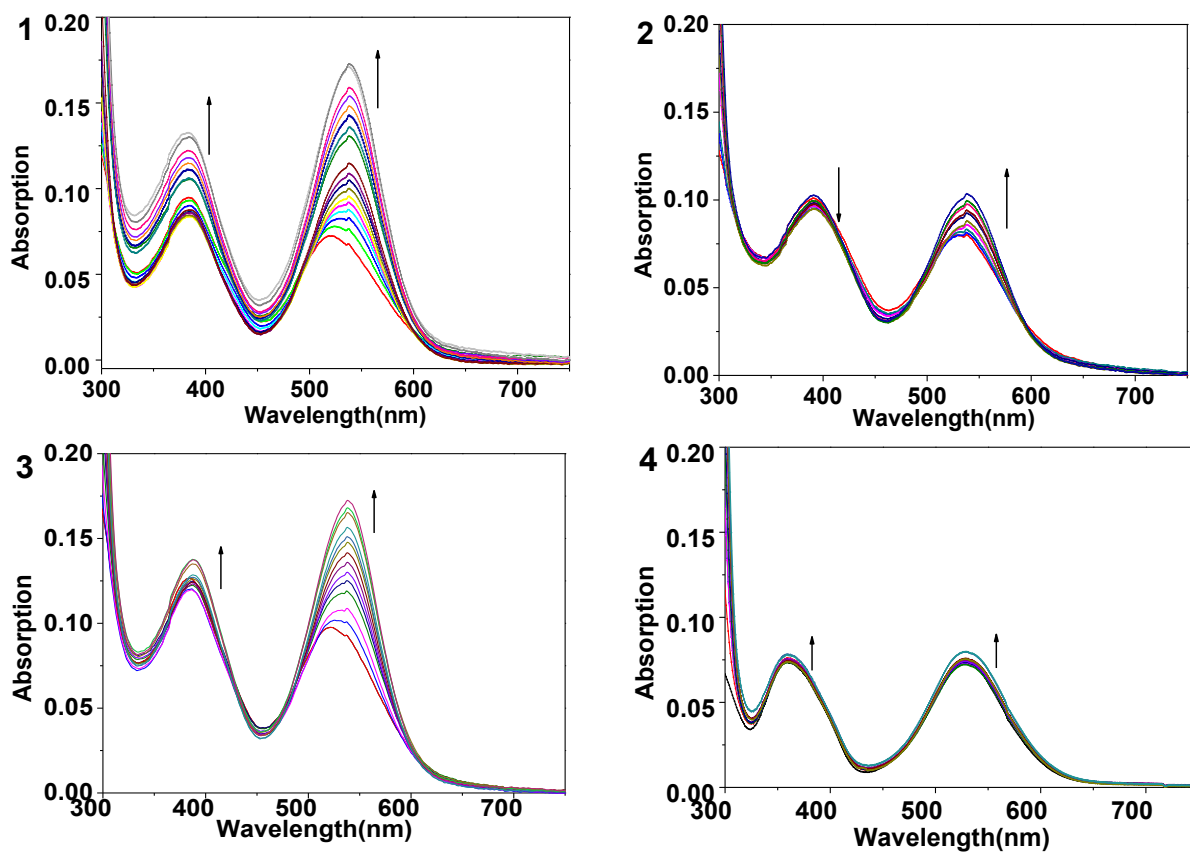
Figure S4. UV-vis titrations of ligands with the telo21 G4-DNA at 25 °C. The final ligand concentration was fixed at 5 μM in a Tris–HCl buffer containing 60 mM KCl. Concentration of telo21 was from 0 to 10 μM.
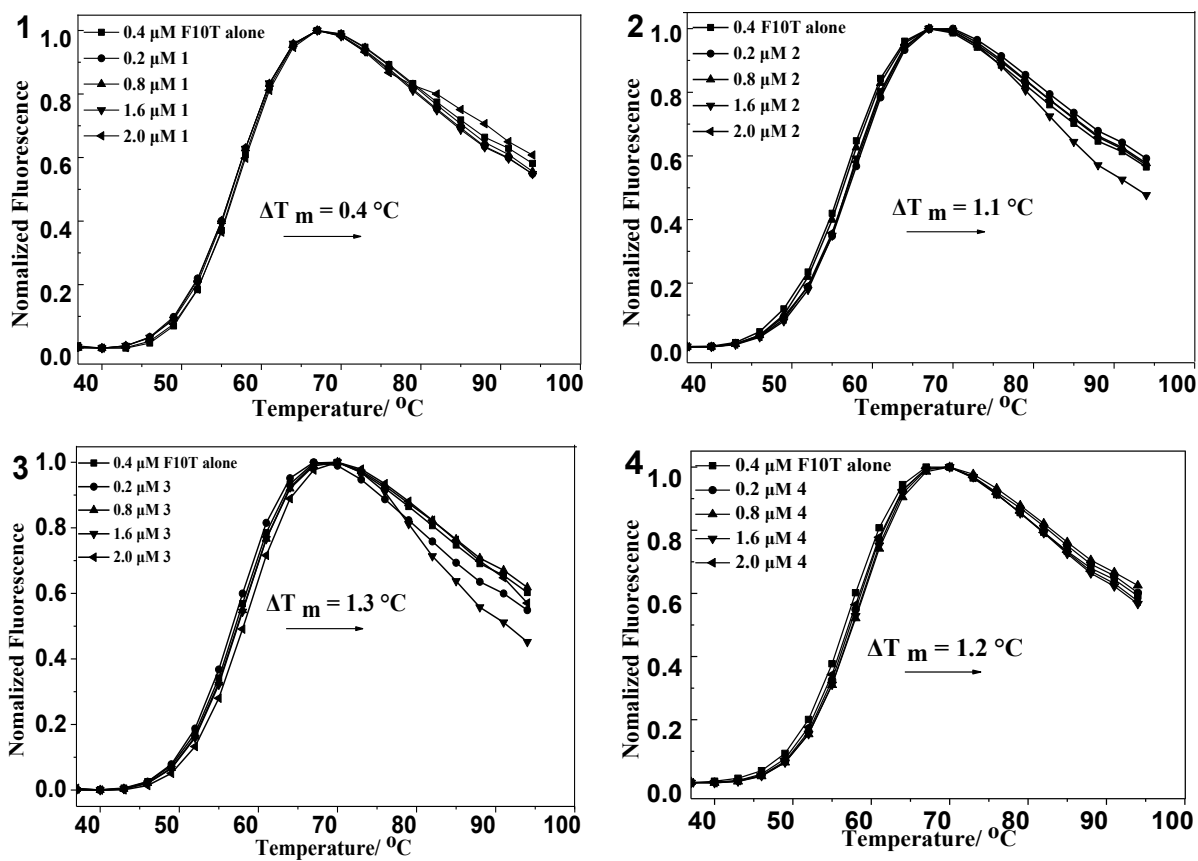
Figure S5. Normalized FRET melting curves of G-quadruplex F10T (0.4 μM) with the addition of different concentration of binding ligands **1-4** (0.2–2.0 μM) in 10 mM Tris–HCl, 60 mM KCl, pH = 7.4.
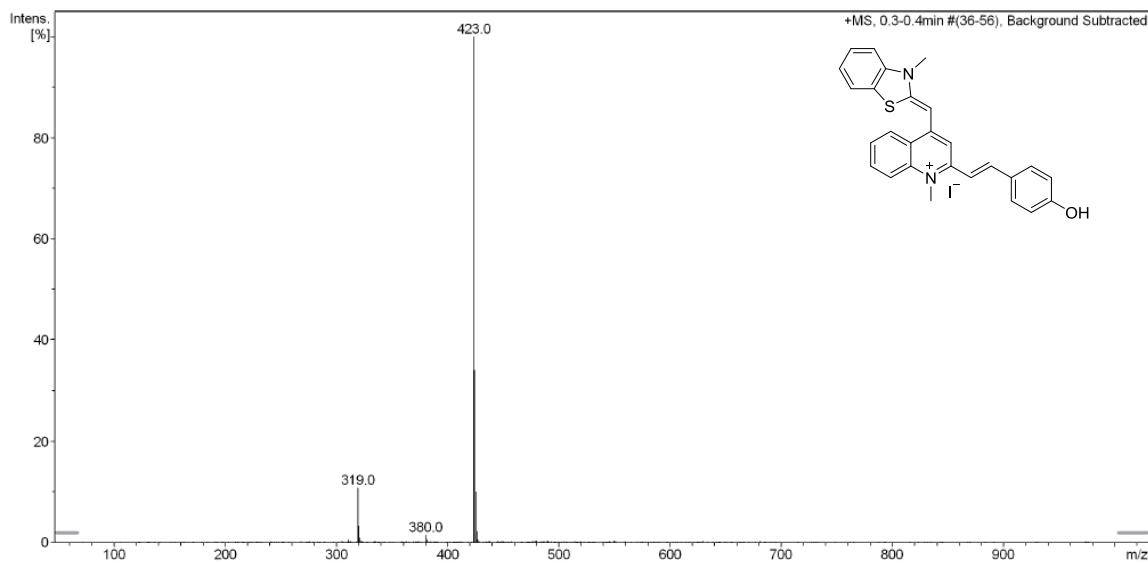
Figure S6-1. ESI-MS of ligand **1**
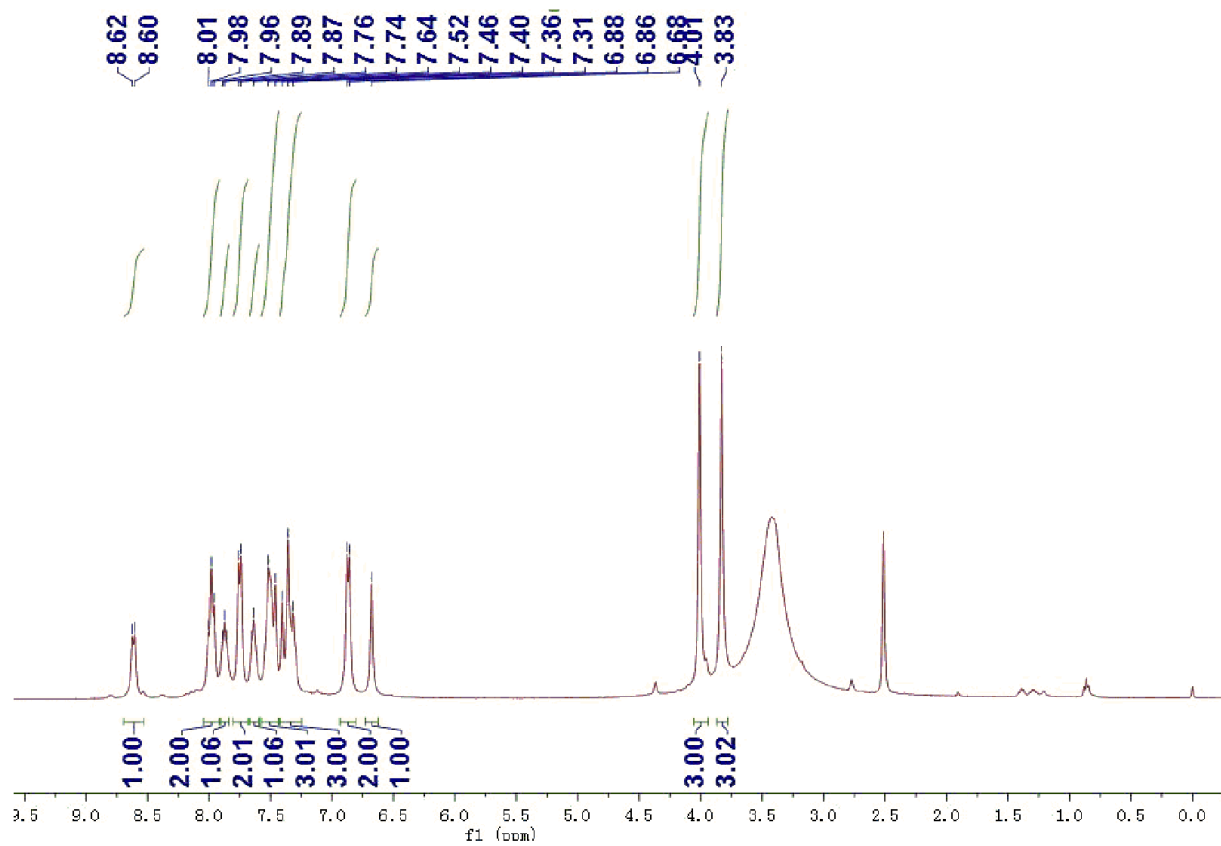
Figure S6-2. ^{1}H NMR spectrum of ligand **1** (DMSO-d_6)
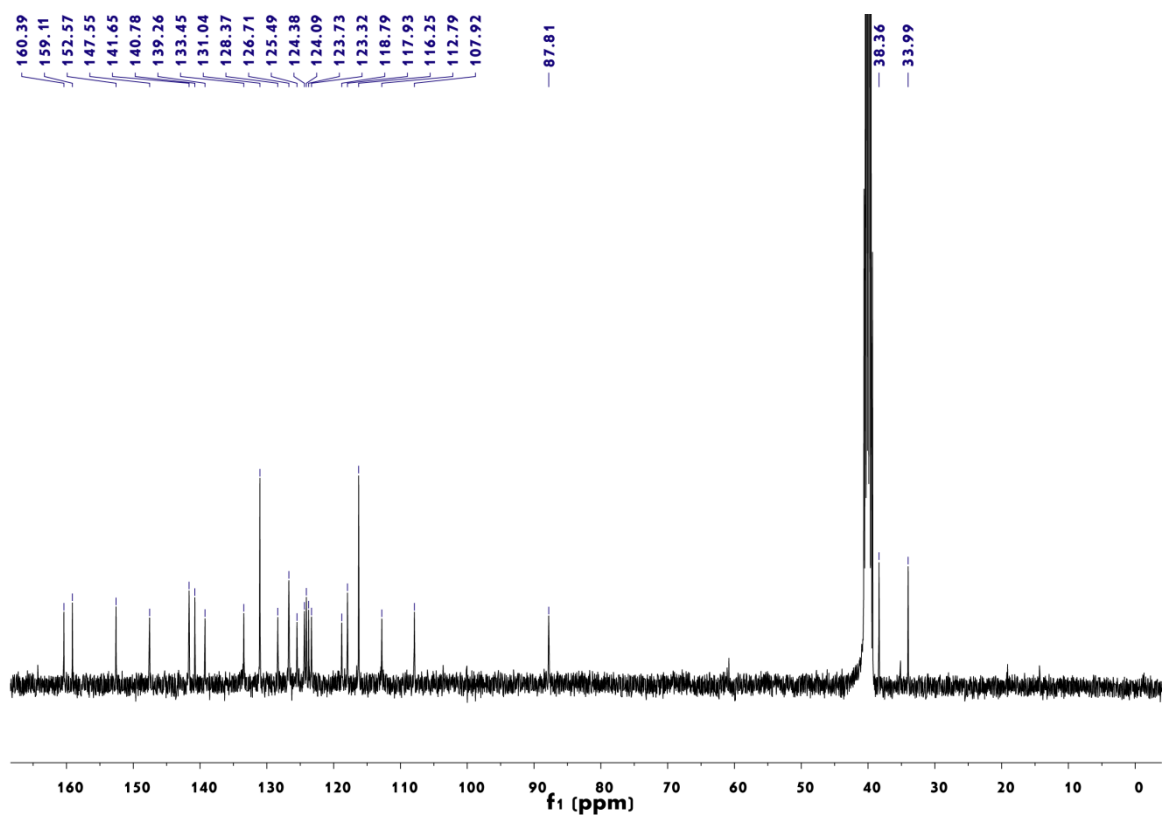
Figure S6-3. ^{13}C NMR spectrum of ligand **1** (DMSO-d_6)
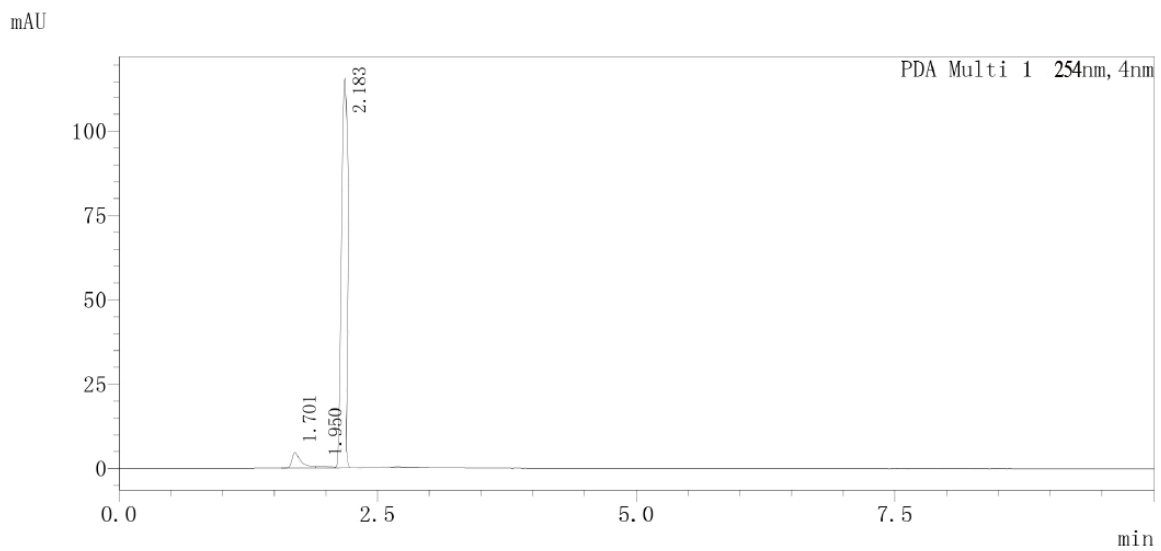
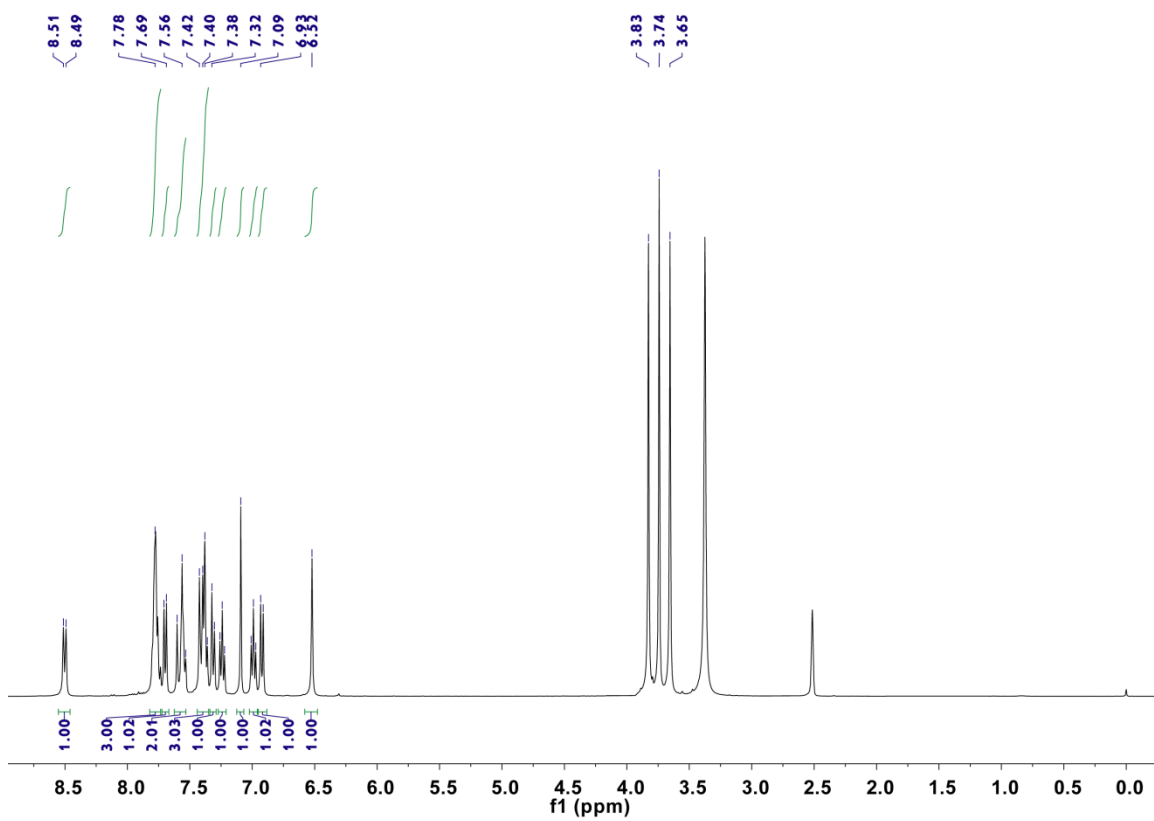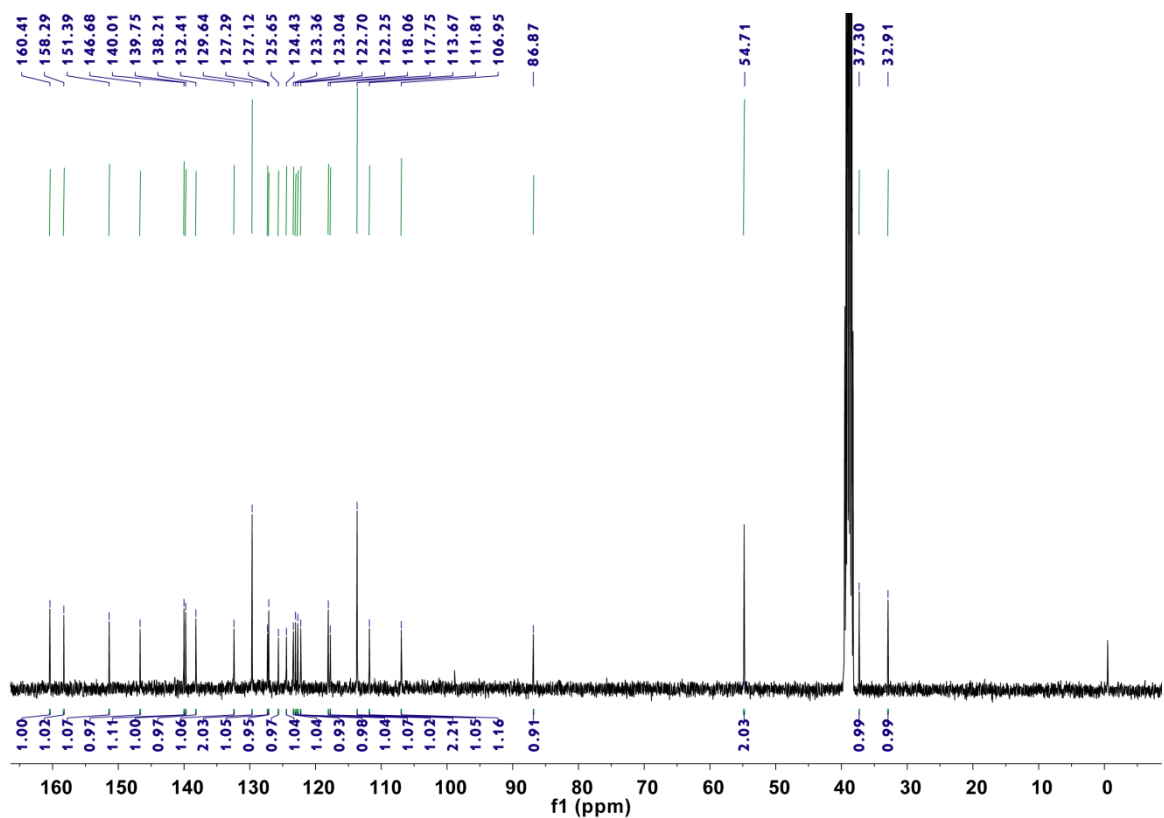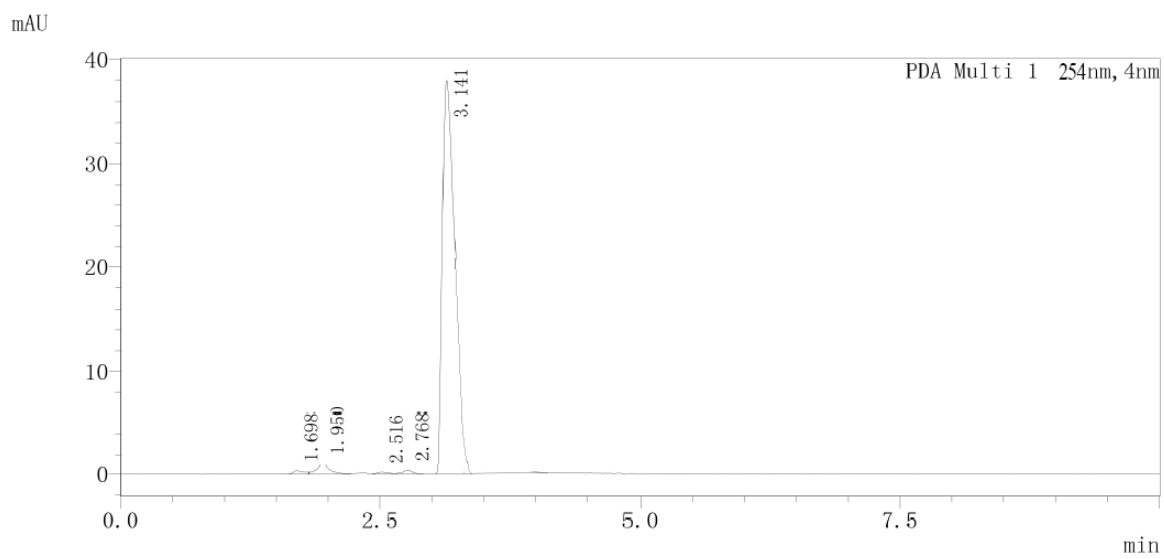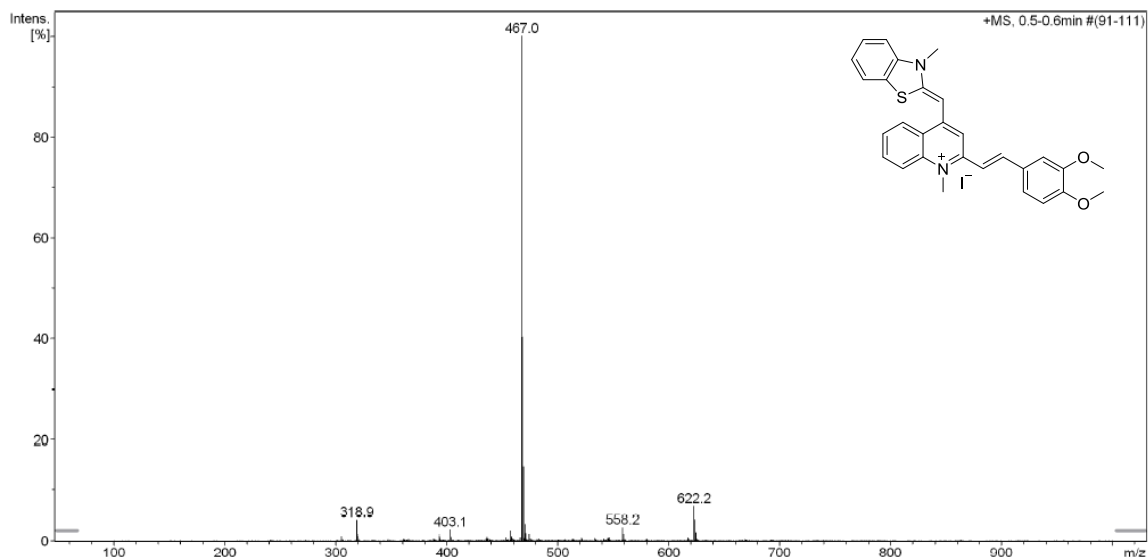Figure S6-4. HPLC analysis of ligand **1**
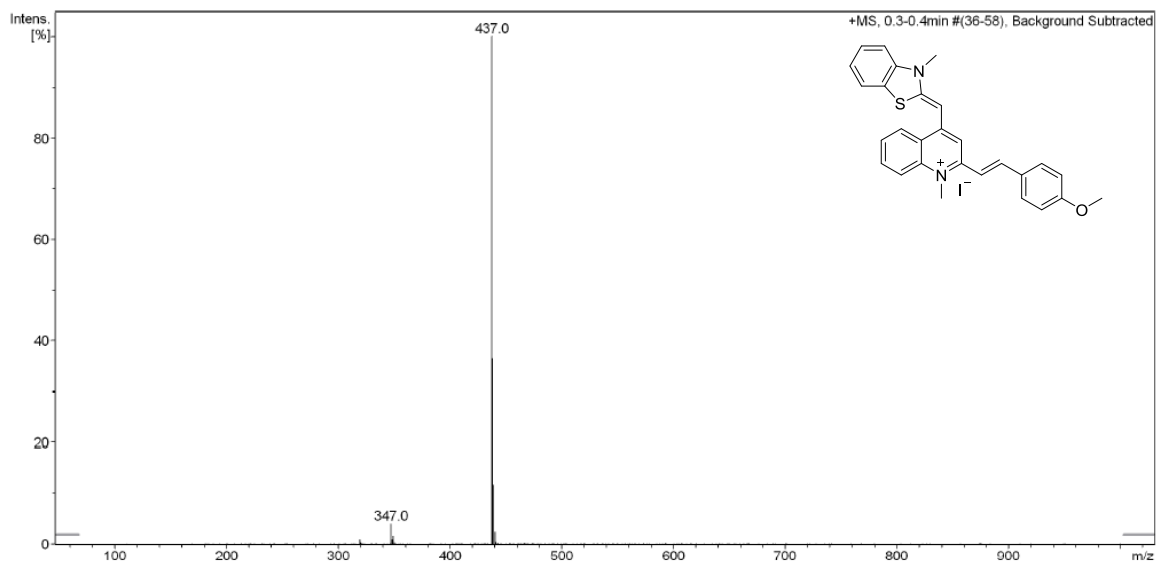
Figure S7-1. ESI-MS of ligand **2**
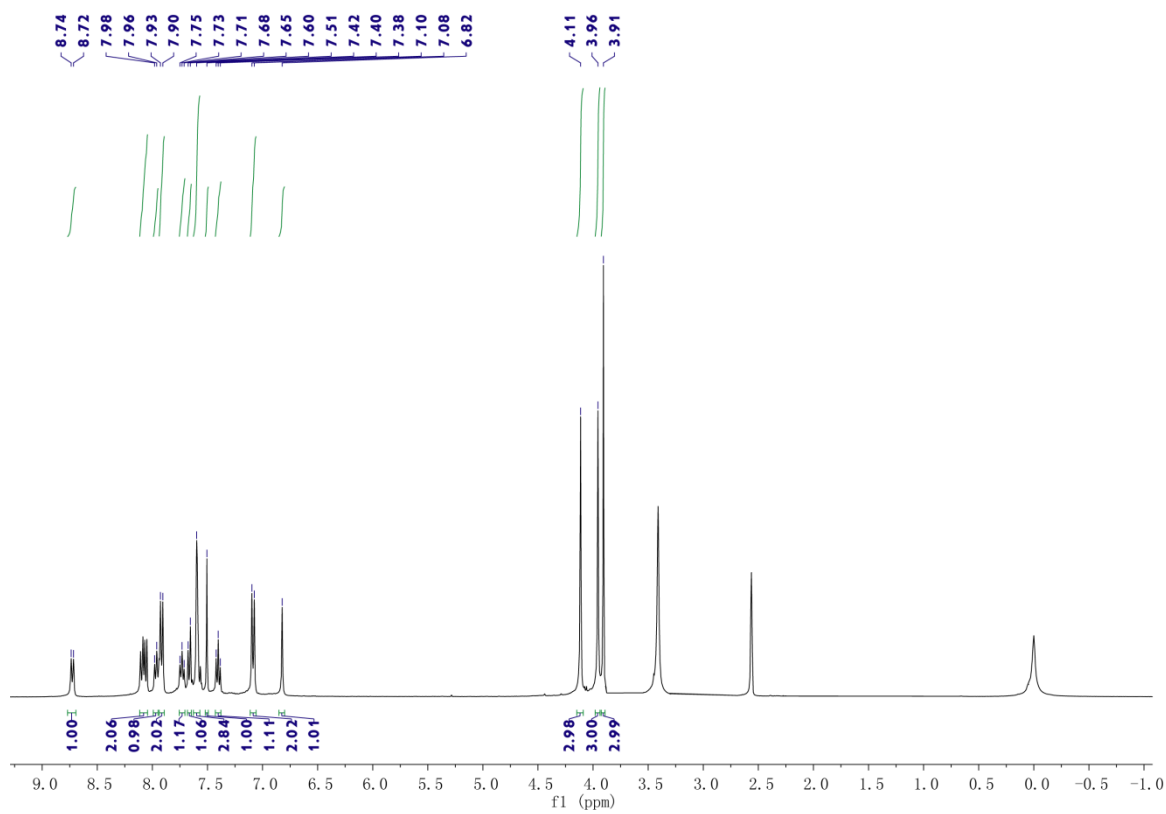
Figure S7-2. ^{1}H NMR spectrum of ligand **2** (DMSO-d_6)
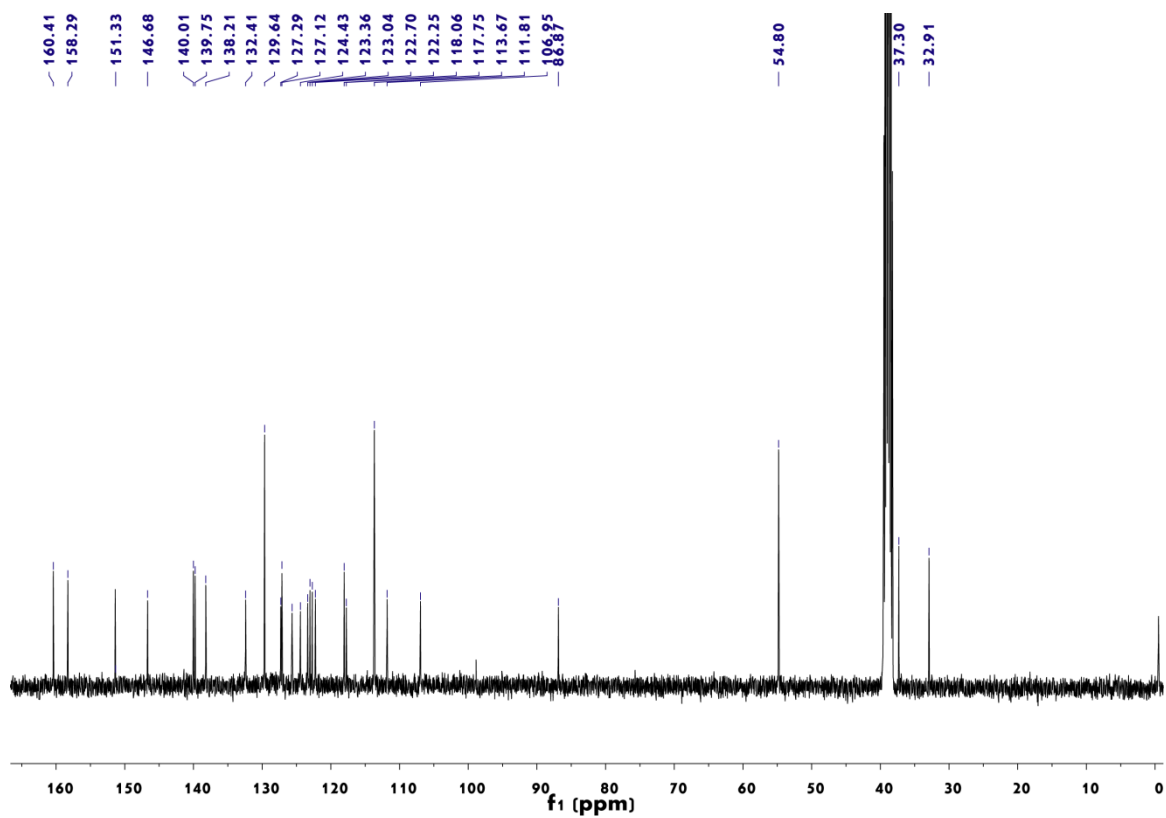
Figure S7-3. ^{13}C NMR spectrum of ligand **2** (DMSO-d_6)
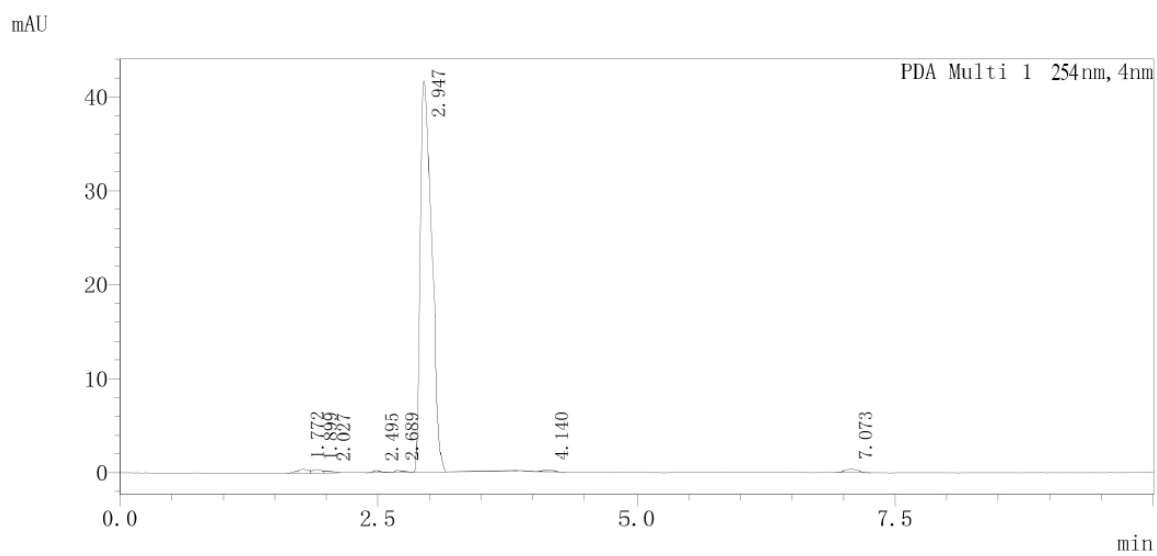
Figure S7-4. HPLC analysis of ligand **2**
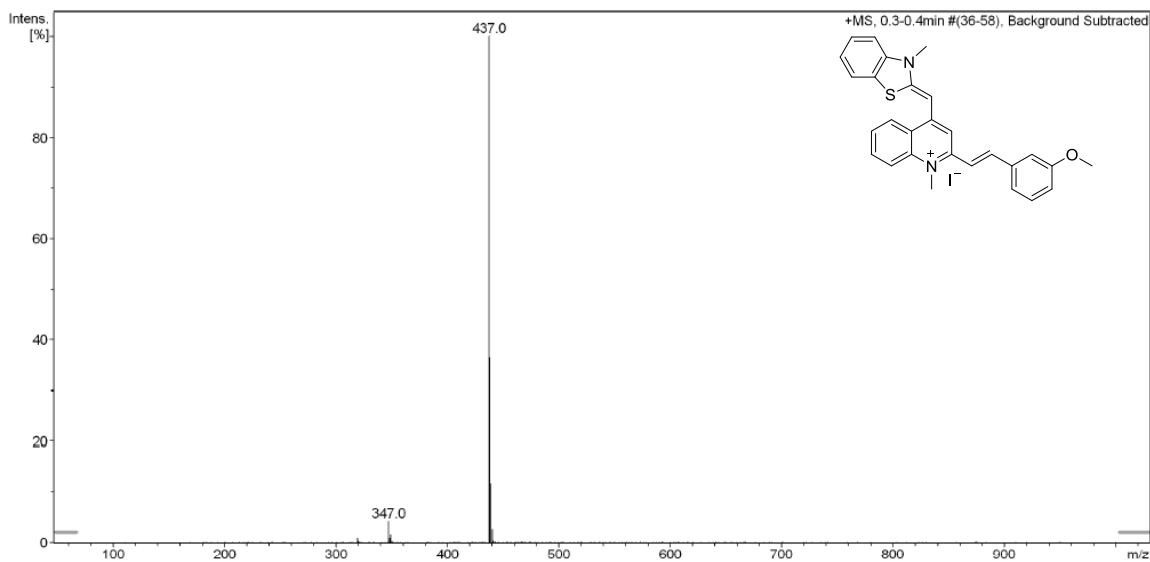
Figure S8-1. ESI-MS of ligand **3**

Figure S8-2. ^{1}H NMR spectrum of ligand **3** (DMSO-d_6)

Figure S8-3. ^{13}C NMR of ligand **3** (DMSO-d_6)

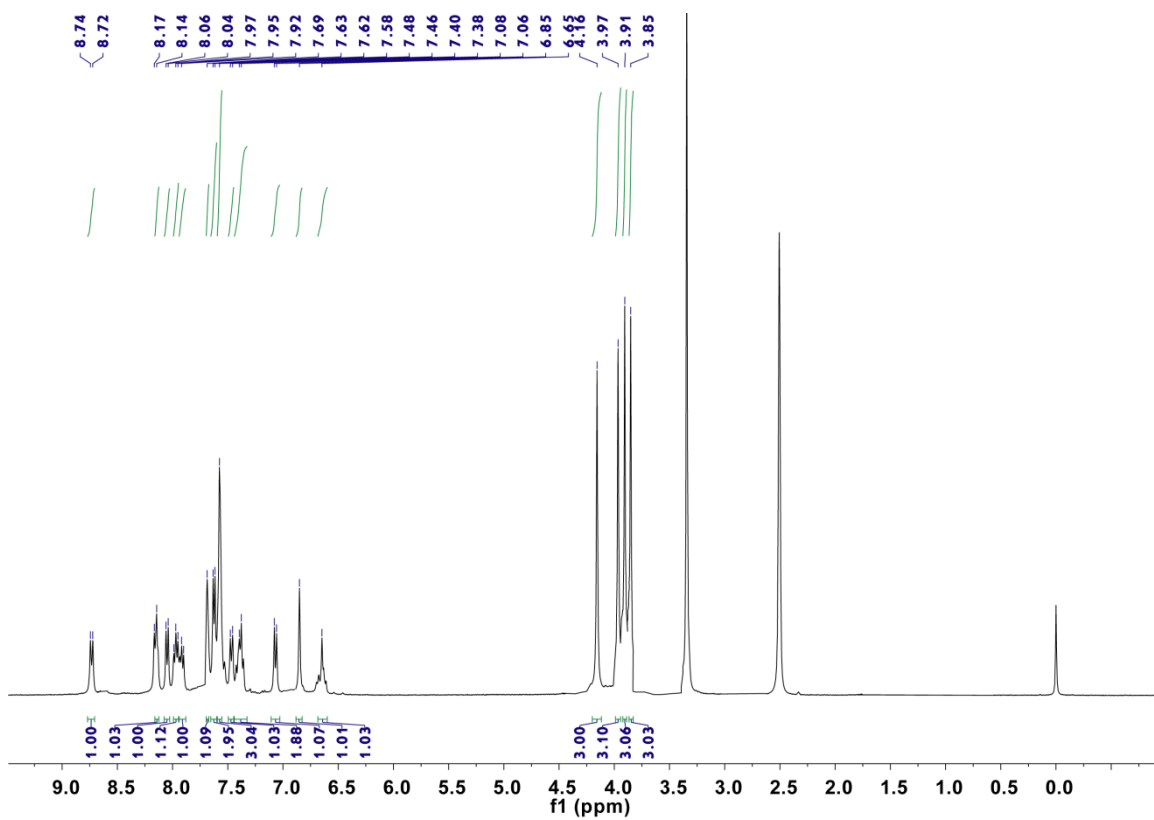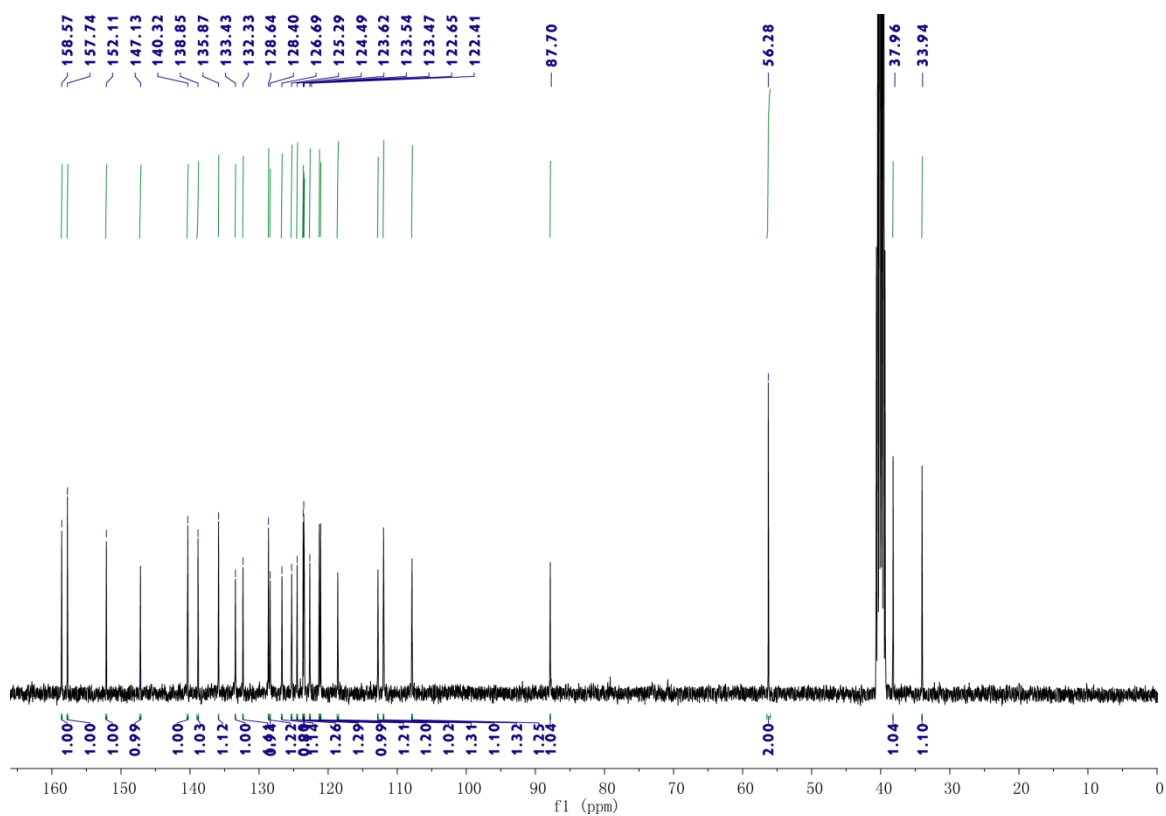Figure S8-4. HPLC analysis of ligand **3**

Figure S9-1. ESI-MS of ligand **4**

Figure S9-2. ^{1}HNMR spectrum of ligand **4** (DMSO-d_6)
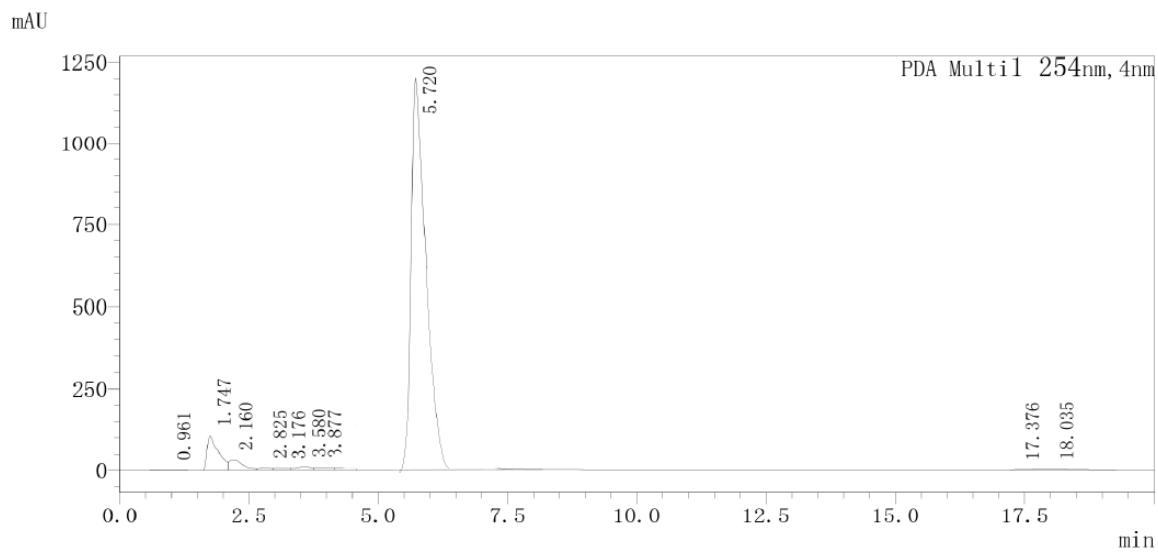
Figure S9-3. ^{13}CNMR spectrum of ligand **4** (DMSO-d_6)

Figure S9-4. HPLC analysis of ligand **4**